PHASE EQUILIBRIUM FOR SOLID AND MOLTEN CeO_{2-x} ABOVE 1500°C

A THESIS

Presented to

The Faculty of the Division of Graduate Studies

by

Michael David Watson

In Partial Fulfillment

of the Requirements for the Degree

Doctor of Philosophy

in the School of Ceramic Engineering

Georgia Institute of Technology

June, 1977

PHASE EQUILIBRIUM FOR SOLID AND MOLTEN

CeO_{2-x} ABOVE 1500°C

Approved:

A. T. Chapman, Chairman

J. L. Pentecost

J. K. Cochran

Date approved by Chairman: May 25, 1977

ACKNOWLEDGMENTS

The author wishes to express his appreciation to Dr. A. T. Chapman for his assistance and advice in the investigation and for acting as chairman of the reading committee. Thanks are also expressed to Dr. J. L. Pentecost and Dr. J. K. Cochran for serving on the reading committee. The typing of the manuscript by Cassandra Harmon and Mary Ann Breazeale is also very much appreciated.

TABLE OF CONTENTS

Chapter Page

LIST OF TABLES

LIST OF ILLUSTRATIONS

Figure Page

SUMMARY

CeO_{2-x} is a nonstoichiometric oxide having a wide solid solution region above 1000°C. The equilibrium between the composition of CeO_{2-x} and the oxygen pressure was determined for solid CeO_{2-x} from 1477°C to 1808°C and for molten ceria from 1850 to 2130°C. Solid ceria was equilibrated with oxygen pressures, 10^{-3} to 10^{-12} atmosphere, in controlled CO/CO_2 gas mixtures. The solid CeO_{2-x} had a continuous solid solution from CeO_2 to $CeO_{1.65}$. The molten CeO_{2-x} was studied with the "internal molten zone technique" to determine the liquidus composition in equilibrium with CO/CO_2 gas mixtures. Liquidus temperatures for CeO_{2-x} were measured and used to calculate the oxygen pressures for the gas mixtures used in the "internal molten zone" experiments. A portion of the liquidus and solidus curves in the CeO_2-Ce_2O_3 system was derived from this information. A phase diagram for the CeO_2-Ce_2O_3 system above 1200°C is presented showing the oxygen isobars for the CeO_{2-x} solid solution and for molten oxide at the liquidus temperatures.

The study demonstrated that the "internal molten zone technique" can be used to investigate the redox equilibrium in nonstoichiometric, molten, refractory oxides. The internal molten zone technique combined with equilibrium data for the

solid at lower temperatures can be used to derive phase diagrams for such oxide systems.

CHAPTER I

INTRODUCTION

Cerium dioxide has one of the higher melting points of the oxides, greater than 2300°C, but it is rarely used as a refractory material. The major disadvantage is that stoichiometric CeO_2 is not stable in an even slightly reducing atmosphere because the dioxide tends to lose oxygen forming substoichiometric CeO_{2-x}. Above 700°C the CeO_2 - Ce_2O_3 system displays solid solution region in which the CeO_{2-x} composition depends upon the temperature and oxygen pressure in the environment.

The phase relations of the CeO_2 - Ce_2O_3 system have been studied below 1500°C by several investigators. At room temperature there are several "so called" intermediate phases with compositions between CeO_2 and Ce_2O_3. At higher temperatures these phases become unstable forming a continuous single phase solid solution region. The equilibrium relations between temperature, composition and oxygen pressure have been investigated up to 1500°C in this region. There has been no investigation of the nature of the solidus and liquidus curves in the system and there is even considerable conflict on the melting points of CeO_2 and Ce_2O_3. The most comprehensive phase diagram extends to only about 1100°C and does not include the equilibrium oxygen pressure information.

The objective of this study was to extend the equilibrium information for solid CeO_{2-x} and the oxygen pressure from about 1500°C to 1800°C and to determine a portion of the solidus and liquidus curves. The data for the solid was obtained by equilibrating CeO_{2-x} in CO/CO_2 gas mixtures of known oxygen potential, quenching, and then analyzing the composition. The liquidus data was determined using the internal molten zone technique in which molten oxide is contained within the interior of a CeO_{2-x} pellet. The experimental data above 1500°C and the literature data were used to draw a phase diagram of the CeO_2 - Ce_2O_3 system including the solidus and liquidus curves and the oxygen pressure information.

The equilibrium information above 1500°C for the ceria system is of great value for the production of certain unidirectionally solidified oxide-metal composites[1]. These composites are produced by a crystal growth procedure employing the internal molten zone technique. The necessary composition of the liquid oxide is obtained by using suitable gas mixture in order to control the nature of the solidified composite.

Ceria has also been recently utilized as additions to refractory oxides, i.e., ZrO_2 in the development of high temperature oxide electrodes for utilization in the search for alternate energy sources such as fuel cells or MHD

facilities. The ceria additions are generally used to improve the electrical conductivity of the insulating oxides and the basic oxidation reduction characteristics of the pure material, CeO_{2-x} are needed as a starting point to evaluate the total stoichiometry affects which are so important in controlling the electronic properties.

CHAPTER II

SURVEY OF LITERATURE

This section is an introduction to nonstoichiometric solids and particularly the CeO_2 - Ce_2O_3 system. The various ceria phases are described and the published phase diagrams presented. The previous studies of ceria are reviewed to show the development of the knowledge of the CeO_2 - Ce_2O_3 system. A section on cyrstal structures describes the phases in the system and the techniques for investigation of equilibrium in molten oxides are reviewed.

Nonstoichiometric Solids

When an element forms cations of different charges and the ionic size does not vary considerably, phases of variable composition exist. Usually intermediate phases also exist, containing some ordered mixture of the two cations. The classic example of this is the iron oxide system in which the ferrous and ferric cations led to the three oxide phases, Wustite FeO_{1+x}, magnetite Fe_3O_{4+x}, and hematite Fe_2O_3.[2,3] Other oxide systems exhibiting this behavior include the metals Ti, U, Zr, Pr, Tb, Eu, Ce, etc.

Cerium forms +4 and +3 cations with radii of 1.01 and 1.11 Å respectively. The oxides formed have the stoichiometric

compositions of CeO_2 and Ce_2O_3. There is a large composition variation at high temperature in the dioxide making the nonstoichiometric formula CeO_{2-x} more meaningful. The sesquioxide also has a composition variation (but not nearly so large) giving the formula Ce_2O_{3+x}. Several intermediate ordered phases also exist at relatively low temperatures with at least one possessing wide composition range.

Solid solution regions around stoichiometric oxide phases are common in metal-oxygen systems in which the metal can form cations of varying charge. The single phase field often has a very narrow composition range, but in some systems the region may possess a widely variable metal to oxygen ratio. The composition within these single phase regions is controlled by the temperature and oxygen partial pressure of the environment. Most phase diagrams which contain such non-stoichiometric oxide phases do not show the equilibrium oxygen partial pressure because of the lack of information. The equilibrium in the systems Fe-O[2,3] and U-O[4,5,6] has been determined and presented on phase diagrams. The equilibrium information is often presented on diagrams with temperature and oxygen pressure axes with isopleths giving the variation in composition[3,4]. The common phase diagram with temperature and composition axes can present the oxygen pressure equilibrium by using isobars[5,6].

Investigations of the Ce-O System

There have been many studies of the Ce-O system but conflicting results and unstudied areas still remain. Initial investigations concerned the existence of the so called intermediate phases or those phases with compositions between CeO_2 and Ce_2O_3. Later attention was turned to the higher temperature solid solution region, CeO_{2-x}. The equilibrium between the oxygen partial pressure and the composition of CeO_{2-x} was investigated. The electrical conductivity and the defect structure of CeO_{2-x} has been of recent interest.

The phase equilibrium relations in the system have been studied at temperatures below 1500°C by several investigators. This section will review their results in chronological order showing the development of the knowledge of the system.

The first studies of ceria involved reducing CeO_2 with hydrogen. Several investigations produced a blue-black product after reduction of CeO_2[7,8]. Meyer[9] concluded this substance was Ce_4O_7. Then Schneck and Roters[10] prepared the blue-black material by controlled reduction of CeO_2 with carbon monoxide and found a single phase with variable composition between CeO_2 and $CeO_{1.90}$. Their results were based on experiments at 700° and 900° and gave the first indication of the solid solution region, CeO_{2-x}. Foex[11] next reported results that again supported the composition of the blue-black materials as Ce_4O_7. Bruno[12] and later Rienacker and

Birkenstedt[13] confirmed the existence of the CeO_{2-x} solid solution by X-ray diffraction techniques. Rienacker and Birkenstedt[13] found the so called "Ce_4O_7" phase to have the same X-ray pattern as CeO_2. Bruno[12] reported that CeO_2 could be appreciably reduced and still retain the fluorite crystal structure with an increase in the unit cell size proportional to the concentration of Ce^{+3} ions in solution. Courtel and Loriers[14] reported a continuous solid solution range between a cubic Ce_2O_3 and CeO_2. Their conclusion was based upon electron diffraction experiments of oxide films on cerium metal.

Brauer and Gradinger[15] studied the CeO_2 - Ce_2O_3 system by annealing many mixtures of the two oxides at 1400°C in nitrogen and then slow cooling over a period of a week. This treatment should yield the phases stable at room temperature if the slow cooling allowed equilibrium conditions to be met. The phases present were identified by X-ray diffraction using a 57.3 mm diameter camera. Their results are shown in Figure 1.

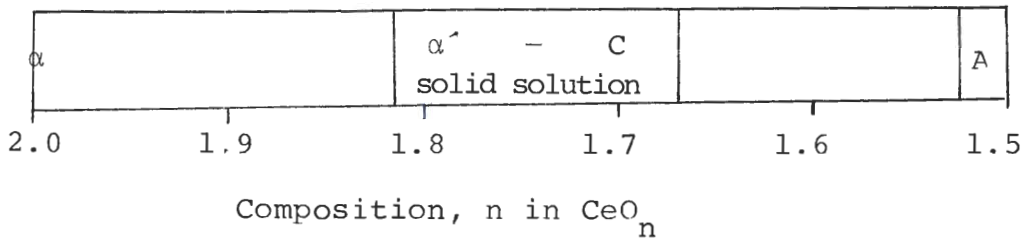

Figure 1. Phases Identified by Bauer and Gradinger[15] in the Ceria System at Room Temperature.

Brauer and Gradinger[15] found four phases in the CeO_2-Ce_2O_3 system. The α phase was stoichiometric CeO_2, having the face centered cubic crystal structure commonly called the fluorite structure. The α´ phase was a nonstoichiometric CeO_{2-x} phase also having the fluorite strucutre. The C phase was another nonstoichiometric phase having a body centered cubic phase. Brauer and Gradinger[15] reported a continuous solid solution between the α´, $CeO_{1.812}$, and the C phase, $CeO_{1.448}$, but they did not have direct experimental evidence to support this. The A phase was hexagonal Ce_2O_3 with a variation in composition from $CeO_{1.525}$ to $CeO_{1.50}$.

The nomenclature used by Brauer and Gradinger[15] and latter authors in naming the A and C phases refers to the "type A" and "type C" rare earth oxide crystal systems. The rare earth sesquioxides form three crystal structures commonly called types A, B, and C. The ceria sesquioxide, Ce_2O_3, forms the hexagonal type A structure and was thus named the A phase. The intermediate phase, C, at about $CeO_{1.67}$ formed the body centered cubic structure called type C structure. Even though this phase was not a true sesquioxide phase, it was given the name referring to this crystal structure. The other phases in the system have been given Greek letters as names. The stoichiometric CeO_2 is α and the nonstoichiometric CeO_{2-x} of the same crystal structure is α´. Other Greek letters were used to name additional intermediate phases found by latter

investigators.

Bevan[16] studied the intermediate phases in the CeO_2-Ce_2O_3 system by X-ray analysis. Samples of various compositions were annealed at temperatures between 800° and 1200°C (the majority at 1050°C) and then quenched to room temperature. The phases present after quenching were determined with a 19 centimeter diameter powder diffraction camera without exposing the sample to air. The gross composition of the sample was then analyzed by oxidation to CeO_2. Bevan believed his quenching technique would retain the phases present at elevated temperature. His results are summarized in Figure 2.

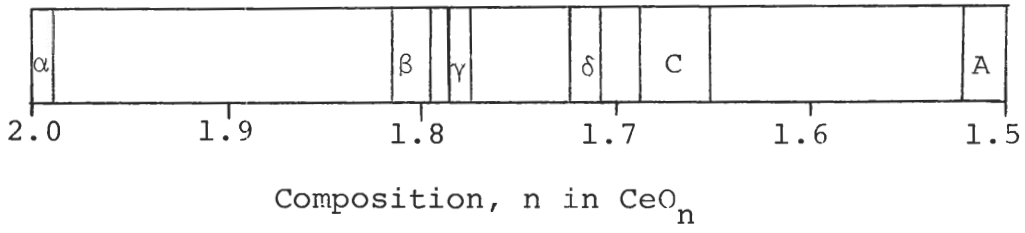

Figure 2. Phases Identified in the Ceria System by Bevan[16]. Samples were quenched from between 800° and 1200°C to room temperatures.

Brauer, Gingerich and Holtschmidt[17,18] investigated the ceria system by high temperature X-ray diffraction and by determining the oxygen partial pressures. They used H_2/H_2O gas mixtures to obtain the very low oxygen pressures necessary. The oxygen pressure-ceria equilibrium is shown in Figure 3. High temperature X-ray analysis with a 12 cm diameter camera

was used to identify the phases present. A phase diagram, Figure 4, was presented for the region CeO_2 - $CeO_{1.78}$. The major feature of this diagram was a solid state immiscibility dome. At room temperature the immiscible phases are stoichiometric CeO_2, α, and $CeO_{1.81}$, the β phase. At about 400°-440°C the β phase transforms from the rhomoohedral crystal structure to the fluorite structure forming the α' phase. From about 440°C to 685°C the two fluorite phases α and α' are the immiscible phases. At 685°C the immiscibility dome closes forming a continuous solid solution region. This single phase region was reported to extend from $CeO_{2.0}$ to $CeO_{1.67}$ at higher temperatures.

Brauer and Gingerich[19] reviewed the various studies of the ceria system and explained some of the inconsistencies in the literature. They stated that the high temperature equilibrium could not be quenched for analysis at room temperature. Thus Bevan's[16] results, Figure 2, do not apply to high temperature equilibrium. In Brauer and Gradinger's[15] initial studies of ceria at room temperature a small X-ray camera was used. This camera could not detect the slight differences between X-ray patterns of the solid solution they reported and the phases, β, γ, and δ, reported by Bevan[16]. Brauer and Gingerich[19] represented the phase relations at three temperatures by Figure 5.

Kuznetsov, Belyi and Rezukhina[20] investigated the ceria

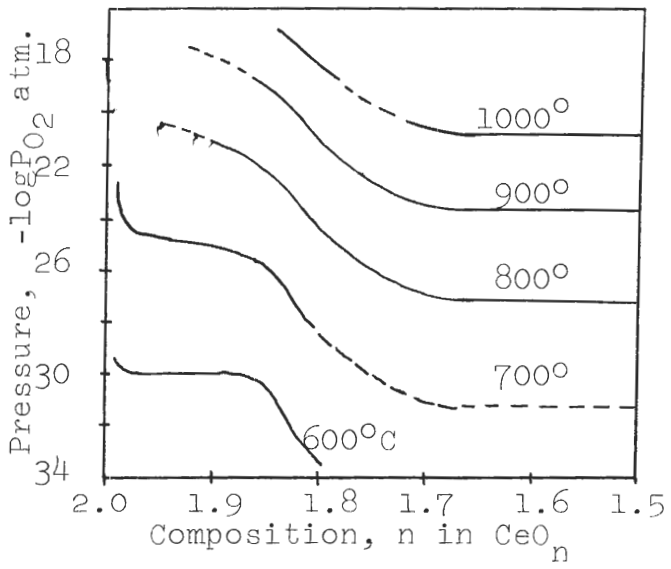

Figure 3. Isotherms for Oxygen Pressure-Ceria Equilibrium by Brauer, et. al.[10,18]

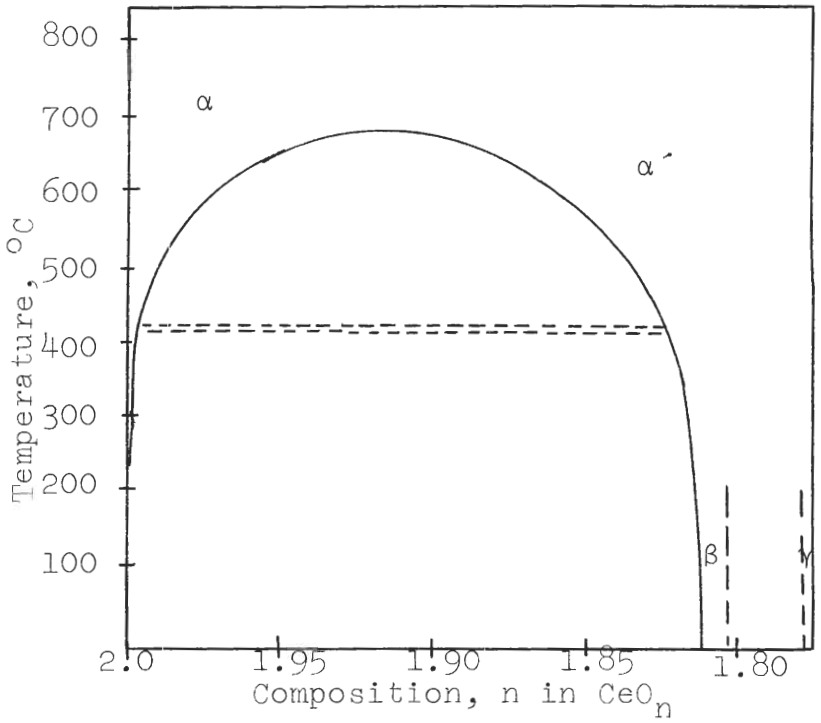

Figure 4. Phase Diagram for the Ceria System by Brauer, et. al.[17]

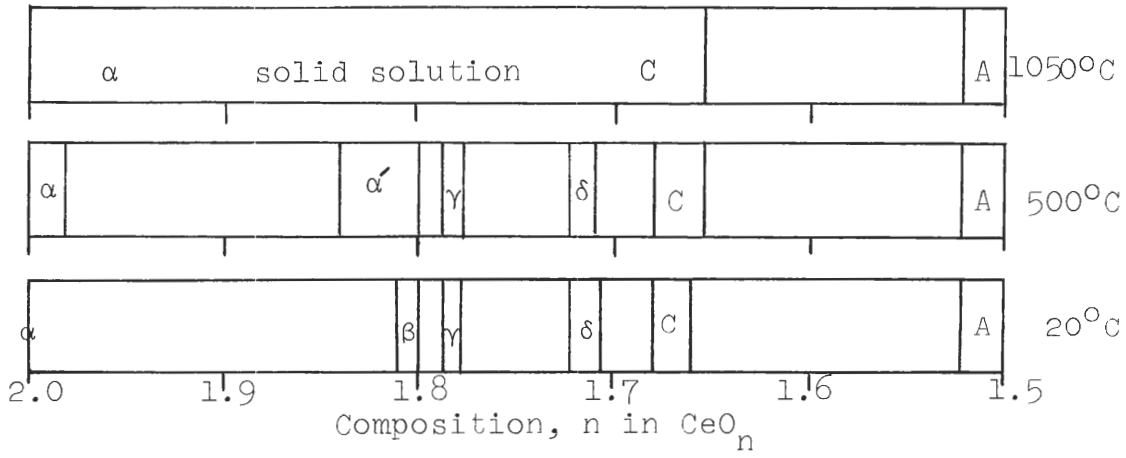

Figure 5. Phase Equilibrium in the Ceria System Reported by Brauer and Gingerich.[19] Unlabeled areas are two phase regions.

system using emf measurements in a galvanic cell and with gas equilibrium measurements. Their experiments were between 700° and 1000°C. A single phase solid solution region was found from CeO_2 to about $CeO_{1.67}$.

Bevan and Kordis[21] studied the ceria system by determining the equilibrium oxygen pressure from 636° to 1169°C using CO/CO_2 and H_2/H_2O gas mixtures. Ceria samples were brought to equilibrium at some known temperature in a flowing gas mixture. The sample composition was determined by in situ direct weighing using a fused-quartz spring. The gas composition was determined by gas-volumetric methods. The results are shown, Figure 6, as isotherms on the composition-oxygen partial pressure diagram.

Bevan and Kordis[21] used their experimental results to derive the phase relations. In Figure 6, areas of two phase equilibrium are indicated by a horizontal isotherm (constant pressure and temperature with a varying composition). Bevan and Kordis[21] used derived thermodynamic data (plots of the free energy versus temperature) to obtain a more detailed analysis of the experimental results. This analysis allowed a correction to be made to the isotherms below 1000°C so that the two phase areas could be better defined. A phase diagram, Figure 7, was then drawn for the system.

The phase diagram, Figure 7, derived by Bevan and Kordis[21], shows a solid solution region at elevated temperatures

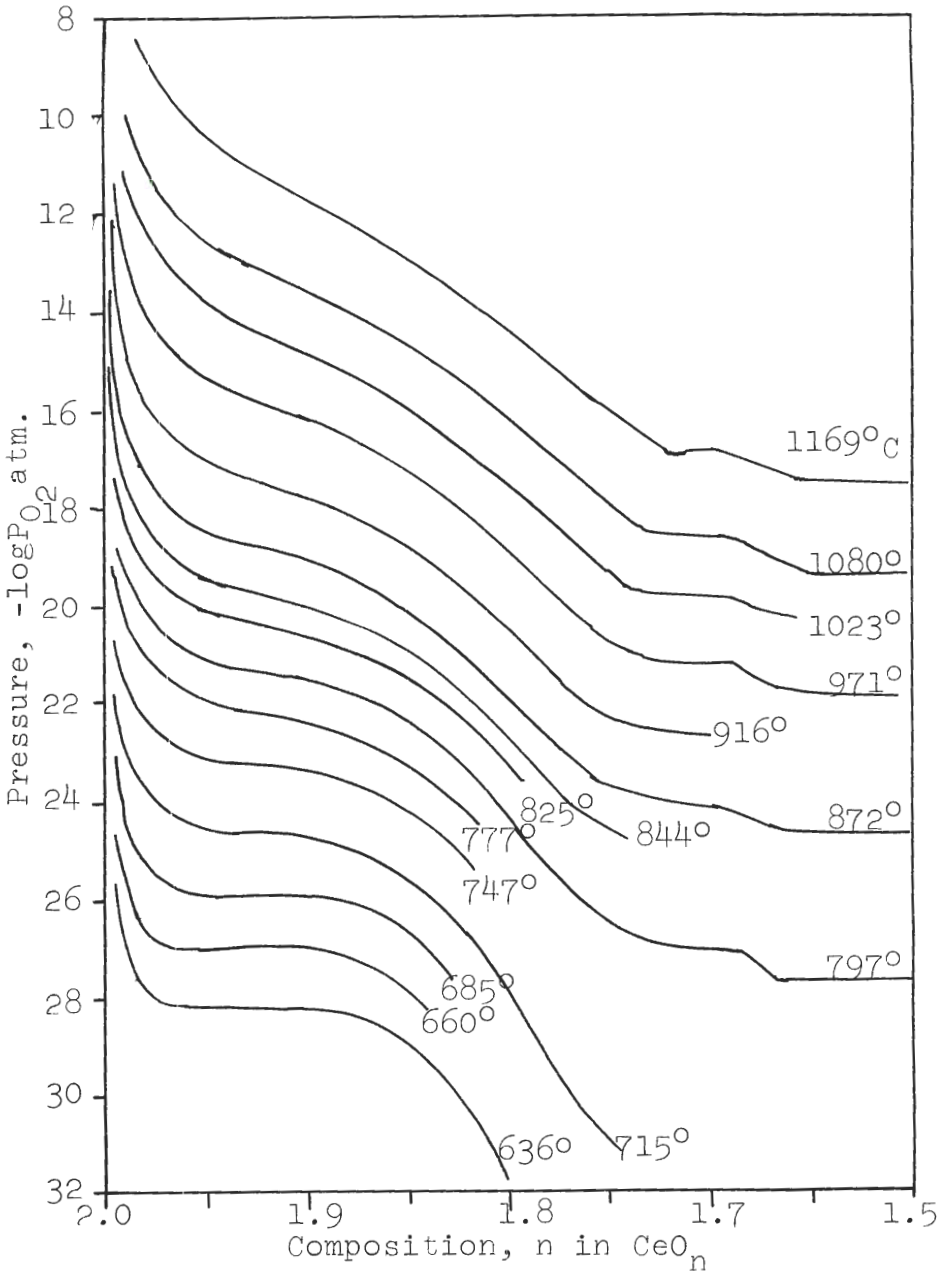

Figure 6. Isotherms for Oxygen Pressure-Ceria Equilibrium by Bevan and Kordis.[21]

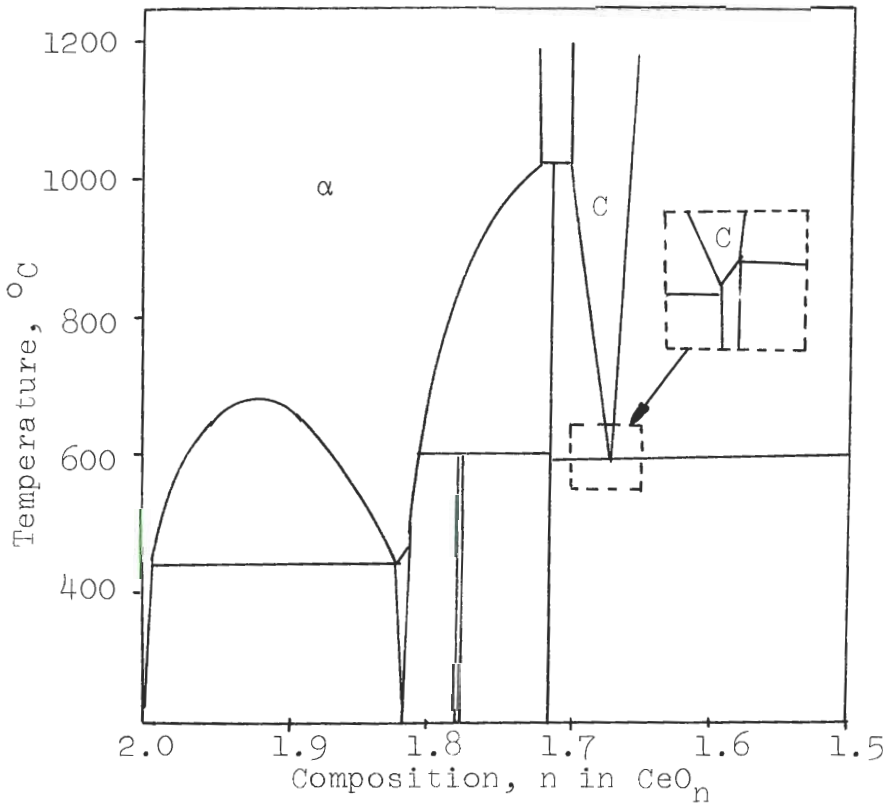

Figure 7. Phase Diagram for Ceria System Derived by Bevan and Kordis.[21] See text for explanation of insert.

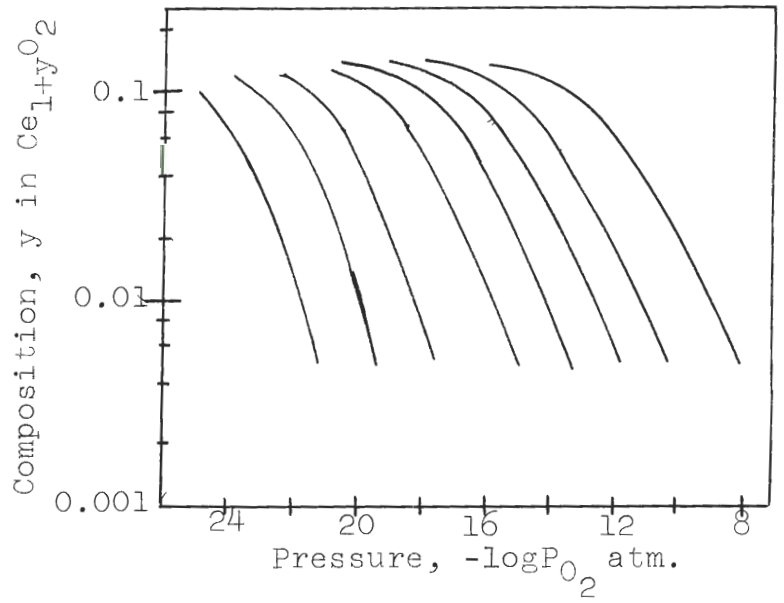

Figure 8. Isotherms for Oxygen Pressure-Ceria Equilibrium Published by Kofstad and Hed[22] from Results of Bevan and Kordis.[21]

and several intermediate phases at lower temperatures. Above 1000°C a two phase region separates the solid solution region from the C phase. Below 600°C the C phase either transforms to an ordered phase or decomposes. Bevan and Kordis[21] did not determine which situation was the equilibrium reaction but showed both possibilities on the diagram by using the insert. The two possibilities for the C phase are described as:

1) The $CeO_{1.67}$ decomposes into $CeO_{1.714}$ and $CeO_{1.5}$ by the eutectoid reaction reaction at 600° as shown in the main diagram;

2) The high temperature disordered $CeO_{1.67}$ orders on cooling at 600° to form an ordered, stoichiometric, phase Ce_3O_5 boarded by the two phase regions shown in the insert to the diagram.

The diagram of Bevan and Kordis[21], Figure 7, is the most comprehensive diagram for the ceria system published to date but it does not contain the oxygen pressure equilibrium information and it conflicts with Brauer[19] and Kuznetsov[20] in the extent of the fluorite single phase region. Above 1023°C Bevan and Kordis[21] report the region extends from $CeO_{2.00}$ to only $CeO_{1.72}$ with even less range at lower temperatures. Above 1023°C they report a two phase region from $CeO_{1.72}$ to $CeO_{1.70}$. Both Brauer and Kuznetsov believe the fluorite single phase region extends into this composition range. Below 1023°C Bevan and Kordis report the ordered phase

$CeO_{1.714}$ with adjacent two phase regions. The essence of the conflict is that Brauer and Kuznetsov both observed a single phase extending across the region that Bevan and Kordis claim contains two phase regions and a low temperature (<1023°) intermediate phase.

Kofstad and Hed[22] used Brevan and Kordis[21] data to investigate the defect structure for CeO_{2-x}. The oxygen pressure data was reploted and presented in the form seen in Figure 8. Kofstad and Hed[22] presented the ceria composition as $Ce_{1+y}O_2$ because they believed the defect structure to consist of interstitial cerium ions. Later studies disagreed with this defect analysis in favor of an oxygen vacancy model.

Ackermann and Rauh[23] investigated the vaporization behavior of the sesquioxide phase Ce_2O_{3-x} and determined the lower phase boundary is the composition of Ce_2O_{3-x} in equilibrium with the liquid metal saturated with oxide. This boundary varies from near Ce_2O_3 at 1327°C to $CeO_{1.34}$ at 1727°C. The oxygen partial pressures were not measured in this system but the partial pressures for Ce and CeO gases were determined over the Ce_2O_{3-x} - Ce_{liquid} system.

Panlener[24] studied the equilibria of CeO_{2-x} from 750 to 1500°C in oxygen pressures of 10^{-2} to 10^{-26} atmospheres. He used thermogravimeteric measurements at these high temperatures in dynamic atmospheres of $CO-CO_2$ and $Ar-O_2$. His results are shown in Figure 9. The single phase region was found to

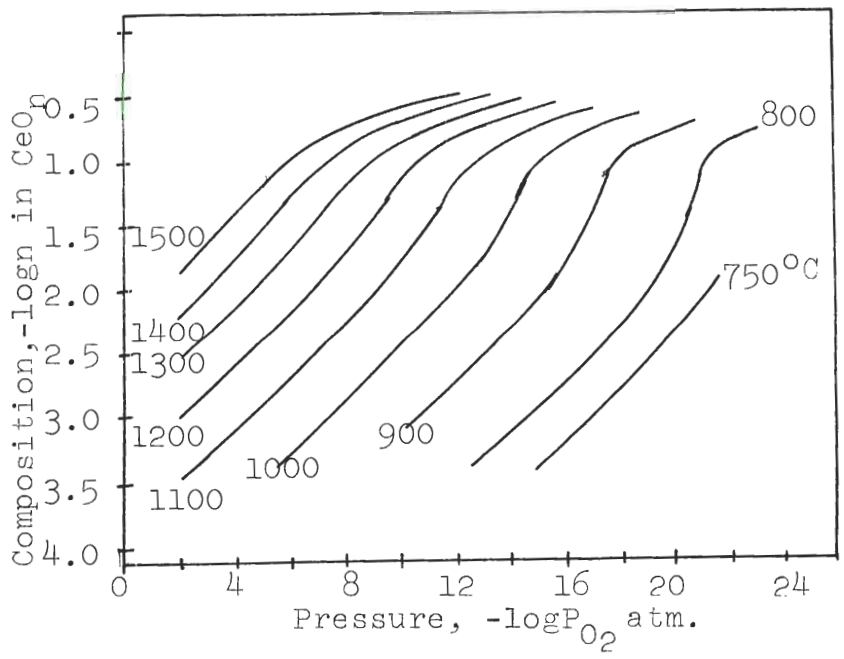

Figure 9. Isotherms for Oxygen Pressure-Ceria Equilibrium by Panlener, et.al.[24,25]

extend over his entire range of composition, $CeO_{2.0}$ to about $CeO_{1.68}$. Bevan and Kordis[21] had reported a two-phase region from $CeO_{1.70}$ to $CeO_{1.72}$ above 1023°C. Paulener's investigation conflicts with Bevan and Kordis at temperatures from 1300 to 1500°C. Below 1300°C, Paulener's data did not extend past $CeO_{1.72}$ into the suspected two-phase region. In a later paper, Paulener, Blumenthal, and Garnier[25] misinterpret Bevan and Kordis[21] regarding the region $CeO_{1.72}$-$CeO_{1.70}$. Paulener, et al., state that Bevan and Kordis observed an ordered single phase between $CeO_{1.72}$ and $CeO_{1.70}$. But in Bevan and Kordis' paper, there are several references to two-phase equilibria in the region $CeO_{1.72}$ to $CeO_{1.70}$. The two investigations do generally agree on the oxygen pressure -- CeO_{2-x} equilibria in the range 800-1200°C, $CeO_{1.95}$-$CeO_{1.73}$. But exact comparisons of the data cannot be made because measurements were not made at the same temperatures.

There have been a number of other investigations of the ceria system, but they were not concerned with phase equilibria. Most of these studies measured the electrical conductivity of pure and doped ceria and analyzed the defect structure of CeO_{2-x}. At present, there seems to be general agreement in the literature that the defect sturcture is oxygen vacancies.

Melting Points of CeO_2 and Ce_2O_3

The melting points of the ceria phases, CeO_2 and Ce_2O_3, have not been well established. Reported temperatures for CeO_2 range from 1950° to 2810°C and for Ce_2O_3, 1687° to 2142°C. Determining the melting point is difficult because of the high temperature involved and occurrence of reactions The ceria will not only react with most refractory holders but also with the atmosphere changing the stoichiometry. To maintain CeO_2, stoichiometric above 2000°C required a highly oxidizing atmosphere while Ce_2O_3 requires a highly reducing atmosphere. Difficulties in obtaining the necessary temperatures and atmospheric conditions have prevented reliable, reproducible determinations of the melting points.

The melting points reported in the literature are given in Table 1 along with information concerning the experimental conditions. Six of the references described the original melting point experiments. The remaining seven references were from tabulated data of melting points and did not list the source of information. Many other references not included here, listed some of the temperatures reported in Table 1 under the original reference. The most common values reported are those of >2600°C for CeO_2 and 1692°C for Ce_2O_3.

Evaluation of the various reported melting points for CeO_2 eliminates several of the values. Ruff's[34] low value at 1950°C was for a sample contaminated with carbon and had an

Table 1. Melting Points Reported for CeO_2 and Ce_2O_3.

Composition	Melting Point °C	Environment	Comments	Ref.	Date
CeO_2	2810	-	*	26	1964
CeO_2	2800	16 atm.	*	27	1949
CeO_2	2750	-	*	28	1960
CeO_2	2725 $\pm$20	-	*	29	1961
CeO_2	>2600	In air heated by O_2-accelylene flame	Did not melt at 2600	30	1931
CeO_2	2600	-	*	31	1973
CeO_2	2480	Air in solar furnace		32	1966
CeO_{2-x}	2397	Ar atmosphere in tungsten tube	Sample partially decomposed	33	1967
CeO_2-C	1950 (1973)**	Packed in ZrO_2 in resistance heated carbon tube	Sample contaminated with carbon	34	1913
Ce_2O_{3+x}	2142	Technical grade H_2	Sample was not completely reduced to Ce_2O_3	33	1967
Ce_2O_3	1692	H_2 atmosphere		35	1925
Ce_2O_3	1690	-	*	28	1960

*These references are surveys that do not list the source of the original information.
**Temperatures after conversion to the "International Practical Temperature Scale of 1948." The original reported temperatures were in the "Geophysical Temperature Scale."

increase in weight during the experiment. Mordovin's[33] value at 2397°C was determined in an argon atmosphere which would result in the reduction of the CeO_2 to a lower oxygen to cerium ratio. Mordovin stated that the solidified material corresponded to the formula CeO_{2-x}, but did not determine the value of x. In a general discussion of refractory oxides, Trombe[27] gave the value of 2800°C for the melting point of ceria and "16 env." (French for atmospheres) but no further explanation nor any reference to the source of the information. The temperatures of 2810°, 2750°, 2725° and 2600°C were found in surveys of melting point data but no references were listed. The 2600°C value was probably meant to be "greater than 2600" referring to Wartenberg and Geurr's[30] study, who could not melt CeO_2 at 2600°C.

Foex[32] found the melting point of CeO_2 to be 2480°C. He used a solar furnace, with an optical pyrometer to measure the melting point of many refractory oxides. The melting points of alumina, 2042°, and zirconia, 2700° - 2710°, were used as reference points to calibrate the pyrometer. Foex's apparatus allowed a black body configuration and prevented contamination by other materials. Solar energy melted a portion of an oxide block creating a cavity partially filled with molten material. With a reduced energy flux, the optical pyrometer was used to measure the cooling curve of the molten oxide. The thermal arrest upon solidification gave the

desired temperature.

The melting point of Ce_2O_3 was determined by Frederich and Sittig[35] as 1692°C and Mordowin, et al.[33], as 2142°C. Two other values, 1690° and 1687°C, were found with no references to the original investigations.

Mordovin, et al.[33], did not measure the melting point for stoichiometric Ce_2O_3 but for a higher oxide, Ce_2O_{3+x}. They annealed CeO_2 rods in technical grade hydrogen at "2000-2200°K" for 10 minutes to produce Ce_2O_3. They could not establish that they had created stoichiometric Ce_2O_3 because the fused material was unstable in air. Because very dry hydrogen and longer time is required to reduce CeO_2 to Ce_2O_3, their fused material was probably oxygen rich, Ce_2O_{3+x}.

Frederich and Sittig[35] found 1692°C as the Ce_2O_3 melting point. They prepared Ce_2O_3 by reduction of CeO_2 in hydrogen, and confirmed the Ce_2O_3 stoichiometry by weight gain upon oxidation to CeO_2. The only question concerning their study is the temperature scale they used. If they used the "Geophysical Temperature Scale" a correction to the "International Practical Temperature Scale of 1948" would bring the melting point to about 1700°C. If they used the "International Scale of 1927," the correction to the 1948 scale would lower the value a few degrees. It is impossible to determine an exact value for the correction because their calibration method was not described. The scale of 1927 was

recognized internationally two years after their publication, but it is possible that it was in use in Germany in 1925.

The two values of 1690°C and 1687°C for the melting point of Ce_2O_3 were found in surveys that did not list the original reference. These values may have been obtained by attempting to correct Frederich and Sittig's[35] value of 1692° by assuming they used the 1927 scale and converting it to the 1948 scale.

The author evaluated the techniques for determining the melting points and believed the most reliable methods were those used by Foex[32] for CeO_2 and Frederich and Sittig[35] for Ce_2O_3. Foex's value of 2480°C for CeO_2 melting point was from a technique that prevented contamination, used an air atmosphere and relied on cooling curves. Other techniques caused contamination or reduction of the sample and relied on visual observation of the liquid formation to detect melting. Frederich and Sittig's value of 1692°C for the melting point of Ce_2O_3 was considered more reliable because they confirmed the oxide composition to be Ce_2O_3. The other technique[33] reviewed did not maintain the stoichiometric composition for the sesquioxide.

Crystal Structures of Phases in the CeO_2-Ce_2O_3 System

The crystal structures of the various phases in the CeO_2-Ce_2O_3 system are briefly described. The knowledge of

these structures is not necessary for a phase equilibria determination, but helps one understand the phase relations. Particularly helpful is the structures of CeO_2 and $CeO_{1.67}$. The existence of a continuous solid solution region between these phases could be explained by the transition from one crystal structure to another by the removal of oxygen ions.

Cerium dioxide, CeO_2, crystalizes in the face centered cubic structure commonly called the fluorite structure. The cerium cation sites are found by a (1/2, 1/2, 0) translation relative to the (0, 0, 0) coordinate. The oxygen anion sites are located by a translation of (1/2, 0, 0) relative to a (1/4, 1/4, 1/4) coordinate. The unit cell contains four CeO_2 molecules and has a lattice parameter of 5.4110 Å. Figure 10 shows this crystal structure of CeO_2.

Cerium dioxide becomes substoichiometric, CeO_{2-x} by the formation of oxygen vacancies[24]. Pascal[36] stated the defective fluorite structure of CeO_{2-x} can have the homogeneity domain of $0 < x < 0.25$ in any of the LO_{2-x} systems where L is any of the lanthanides Ce, Pr, or Tb. The CeO_{2-x} structure was studied by Brauer and Gingerich[17] with high temperature X-ray diffraction. They found at 900°C a continuous linear variation in the face centered cubic lattice parameter from 5.41 Å for $CeO_{2.0}$ to 5.56 Å for $CeO_{1.67}$.

The intermediate phase around $CeO_{1.67\pm x}$ was reported by Bevan[16] to crystalize in a body centered cubic structure com-

monly called the type C rare earth oxide structure. The lattice constant varied continuously from 11.107 A for $CeO_{1.688}$ to 11.126 A for $CeO_{1.651}$. Bevan used room temperature X-ray diffraction techniques to analyze samples quenched from 1050°C and believed the quenching retained the high temperature crystal structure. Brauer[19] later stated that the high temperature crystal structure could not be quenched to room temperature.

Suchet[37] explained that a continuous translation from the fluorite structure of CeO_2 to the type C structure of $CeO_{1.67}$ reported by Bevan[16] is possible by the removal of oxygen ions. The type C structure is a overstructure of the defective flourite structure if a quarter of the oxygen ions were removed from the stoichiometric flourite phase. Figure 11 shows the type C structure for a stoichoimetric L_2O_3 that crystallizes in this structure (L represents any rare earth element). Dotted circles in Figure 11 show the sites of the oxygen ions removed from the flourite structure and the dotted cube represents a flourite unit cell. Suchet believed that continuous solid solutions between phases of these different crystal structures were explained by this overstructure concept. He stated that many solid solutions between the oxides LO_2 and L'_2O_3 (L and L' represent two different lanthanide type elements) exist because of this translation of crystal structures. The solid solution between CeO_2 and $CeO_{1.67}$ was

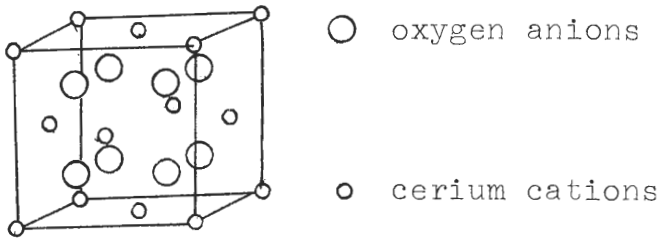

Figure 10. The Face Centered Cubic, Fluorite, Crystal Structure of CeO_2.

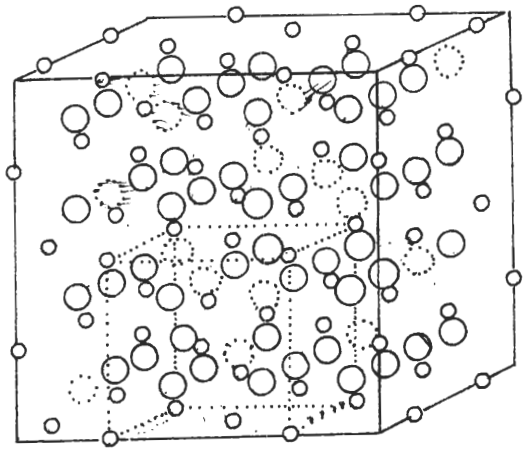

Figure 11. The Body Centered Cubic, Type C, Crystal Structure of Rare Earth Sesquioxides. The solid circles represent the oxygen anions in a stiochiometric sesquioxide.The dotted circles are the oxygen anions withdrawn from the fluorite structure to derive the type C structure. The dotted cube represents a flourite unit cell

also explained by this translation by considering $CeO_{1.67}$ as Ce_2O_{3+x}. If some of the vacant oxygen sites (represented by dotted circles in Figure 11) were occupied, the type C structure would describe the $CeO_{1.67}$ phase.

The sesquioxide, Ce_2O_3, forms the hexagonal, type A, rare earth oxide structure. This structure which is found in many L_2O_3 lanthanide series oxides. Bevan[16] reported lattice constants of a = 3.889 $\pm$ .002 and c = 6.054 $\pm$ .002 for the composition $CeO_{1.522}$ which is within the Ce_2O_{3+x} composition range.

The three low temperature ordered phases have the rhombohedral or hexagonal strucutre. The β phase at $CeO_{1.81}$ is formed by the ordering upon cooling at about 400°C of the α' fluorite phase. This structure is derived from eight unit cells of CeO_2 by the creation of six anion vacancies. Bevan[16] reported the lattice constants of a = 3.890 and c = 9.536 for β; $CeO_{1.812}$. The γ phase $CeO_{1.778}$, has the lattice constants of a = 3.910 and c = 9.502. The δ phase, $CeO_{1.717}$, has the constants of a = 3.921 and c = 9.637.

Techniques for Studying Redox Equilibrium in Molten Oxides

The evaluation of the reduction-oxidation (redox) equilibrium in molten oxides has previously been determined in only two systems, Fe-O[3] and U-O[5]. The techniques used in these investigations are discussed in this section. The methods are

reviewed for consideration of their application to the Ce-O systems.

Darken and Gurry[3] studied the Fe-O system by using a variety of techniques. The equilibrium between molten oxide and oxygen was determined by a procedure that maintained molten oxide at a constant temperature in a flowing gas mixture of known oxygen partial pressure. After equilibrium was attained the material was quenched and the oxide composition analyzed. An extensive series of experiments varied the temperature between 1380° and 1640°C and the oxygen pressure from one atmosphere to log Po_2 of -10. The temperature range was low enough to use a platinum wound resistance tube furnace. The molten oxide was contained in platinum crucibles. Platinum solubility in the molten oxide was low enough to avoid any measurable effect on the results. But the use of platinum crucibles was limited by absorption of iron from the sample. The crucibles became Pt-Fe alloys with the melting point decreasing as the iron content increased. Thus the crucibles were limited to temperatures much below the melting point of pure platinum.

Darken and Gurry[3] determined the liquidus and solidus lines of wustite, FeO_{1+x}, and magnetite, Fe_3O_{4+x}, by the following technique. An iron wire was suspended in a flowing gas mixture at a constant temperature slightly below the suspected melting point. The iron was converted to an oxide

with a composition determined by the atmosphere and the temperature. The sample was cooled and visually examined. If there was no evidence of melting, the sample was reheated to a slightly higher temperature in the same gas mixture. This procedure was repeated until the melting point of the oxide in equilibrium with the gas mixture was found. The oxide composition corresponding to the measured melting point and oxygen pressure in the gas mixture was derived from appropriate graphs. Composition-temperature-oxygen pressure information measured for the solid at much lower temperatures was extrapolated to the melting points to determine the solidus compositions. The liquidus compositions were obtained from similar graphs of equilibrium determined for the molten oxide. By measuring the melting points of oxides in eleven gas mixtures and deriving the oxide compositions, Darken and Gurry[3] established the liquidus and solidus lines for wustite and magnetite in the Fe-O system.

An investigation of the redox equilibrium in molten $UO_{2\pm x}$ was performed by Chapman, Brynestad, and Clark[5]. They determined the equilibrium oxygen partial pressure for molten $UO_{2\pm x}$ at the liquidus temperature and for solid UO_{2+x} at 1660°C. These results were combined with literature data for equilibrium oxygen pressures from 1200° to 1500°C and the known liquidus and solidus lines to construct a phase diagram from 1200° to 2900°C for $UO_{2\pm x}$ including the oxygen isobars.

The technique used for studying molten $UO_{2\pm x}$ was known as the internal molten zone technique. Cylindrical UO_2 pellets were heated by induction heating at 3.5 megahertz. A zone of molten oxide was contained within the interior of the pellet by the solid skin which was cooled by thermal radiation losses. The pellet was exposed to a flowing gas mixture until the composition of the oxide equilibrated with the oxygen pressure in the gas mixture. The pellet was quenched and the resolidified interior analyzed to determine the liquid composition. A series of experiments established liquid compositions for nine different gas mixtures.

Chapman, et al.[5], believed the temperature of the molten oxide could not vary significantly from the liquidus temperature which was assumed to be approximately 3150°K for all experiments. This temperature was used to calculate oxygen pressures for the gas mixtures. The oxygen pressures and corresponding liquid compositions were believed to represent equilibrium conditions for the liquidus line in the phase diagram.

The major difficulties in using the internal molten zone for determining phase equilibrium are the presence of very large thermal gradients in the solid skin and the absence of any direct temperature measurements. Chapman, et al.[5], discussed these problems and justified the use of the liquidus temperature for calculating the oxygen pressure. The internal molten zone technique provided a method for attaining a very

high temperature while containing the molten oxide without contamination from a crucible. The technique had problems in precisely defining the equilibrium conditions in the system but no other method has been demonstrated that can be used to determine equilibrium in molten oxides above 2000°C.

CHAPTER III

EQUIPMENT AND PROCEDURE

This chapter describes the equipment and procedures used for determining the redox equilibrium in the CeO_2-Ce_2O_3 system. The first section describes the equipment used in all phases of the investigation and latter sections describe different portions of the procedure. The first portion of the procedure concerns the temperature calibration of the furnaces. The next section is the procedure for determining equilibrium between solid ceria and oxygen at temperatures from 1477° to 1808°C. The internal molten zone technique and the determination of melting temperatures are described in separate sections which both concern the liquidus equilibrium information. The final two sections cover calculation of oxygen pressures and the determination of CeO_{2-x} compositions. These two sections are important for both the solid and the molten CeO_{2-x} equilibrium experiments.

Equipment

The redox equilibrium experiments for both solid and liquid CeO_{2-x} were performed in the induction furnace shown schematically in Figure 12. A smaller induction furnace, shown schematically in Figure 13, was employed for determining

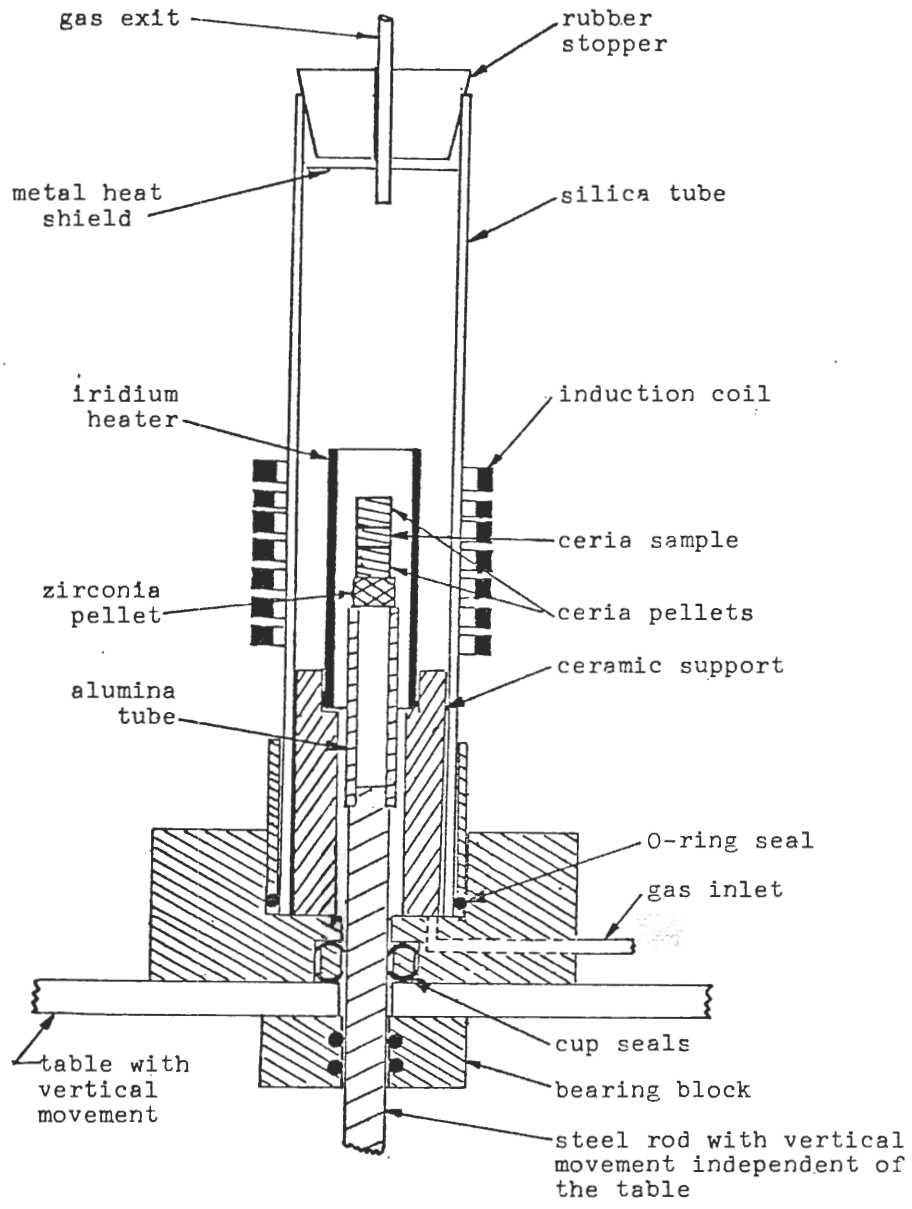

Figure 12. The larger induction furnace.

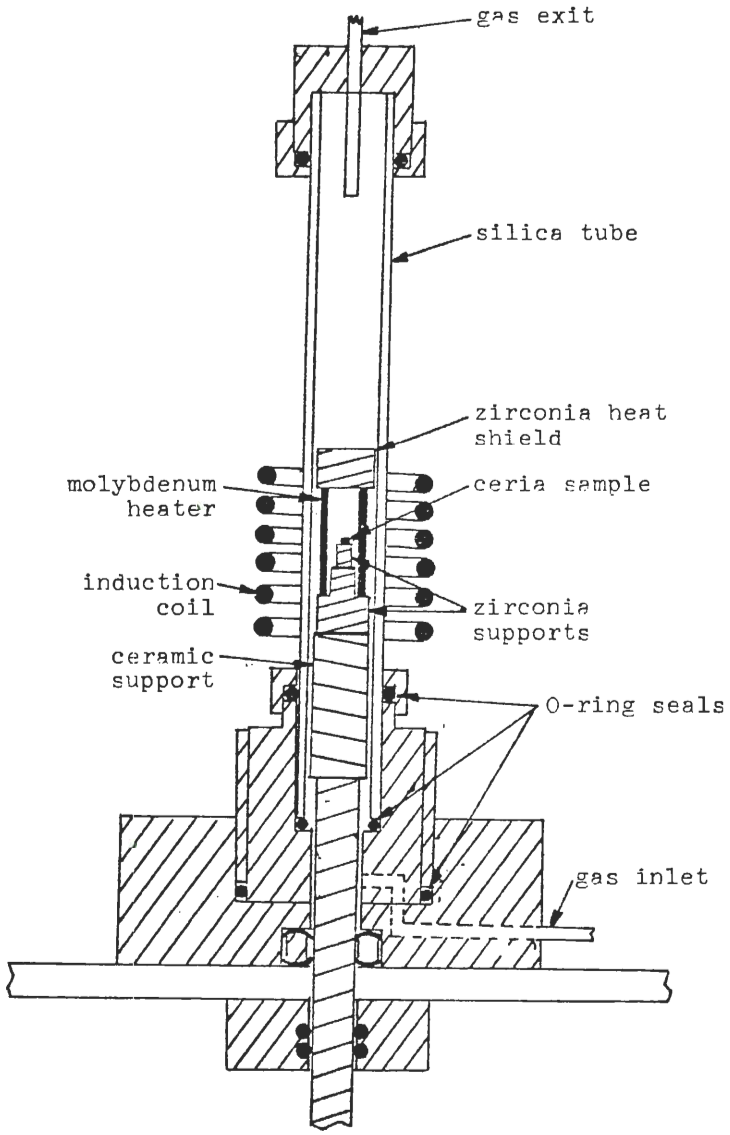

Figure 13. The smaller induction furnace for determining melting points.

the melting temperatures for CeO_{2-x} in selected oxygen pressures. These two furnaces could be used interchangeably with associated apparatus for control and analysis of the atmosphere.

The larger induction furnace shown in Figure 12 consisted of a fused quartz tube 38 millimeters in diameter enclosing the sample, refractory supports, and a iridium metal susceptor tube. The iridium tube was heated by induction heating by the external induction coil. The power was supplied by a 10kw Lepel high frequency generator operating at 3.6 megahertz. Iridium was used as the susceptor because it does not react with the CO/CO_2 atmosphere used to establish controlled oxygen pressures. The CeO_{2-x} sample was supported by a column consisting of a zirconia pellet, alumina tube, and a steel rod. The iridium tube was supported by an alumina refractor and the furnace base so that it was concentric to the sample column. The furnace was constructed so the iridium tube could be moved vertically, independent of the sample, while an experiment was in progress. This motion was necessary for the molten CeO_{2-x} experiments in which the sample was first preheated within the iridium tube. The iridium tube was then lowered exposing the sample pellet to the electro-magnetic field allowing additional heating and subsequent internal melting.

The smaller induction furnace, Figure 13, was similar to the large furnace, but allowed movement of only the 15 millimeter diameter fused quartz tube. When vapor deposits

on the quartz tube hindered accurate temperature measurements by the optical pyrometer the quartz tube could be adjusted to allow viewing through a clean portion of the tube. The ceria sample was supported on zirconia and remained stationery within the molybdenum susceptor tube. The smaller susceptor tube could be heated to much higher temperatures making possible the measurement of the heating points of selected CeO_{2-x} compositions. The ends of the tube were slotted to allow flow of the CO/CO_2 gas mixture to the sample. However, the molybdenum could not be used in CO/CO_2 atmospheres containing over 10% CO_2 without oxidizing. A small diameter iridium tube would have alleviated this problem but it was not available.

The gas control system, shown schematically in Figure 14, provided the CO/CO_2 gas mixtures and controlled oxygen potentials used during all the experiments in both induction furnaces. The system typically was evacuated prior to admitting controlled CO/CO_2 mixtures. An analysis of the inlet or exhaust gas mixture was obtained with the gas chromatograph. Accurate measurements of the flow rates of either CO or CO_2 before their mixing were obtained with the burette flow meter.

The gas chromatograph was usually used to analyze gas mixtures to determine when equilibrium was attained in the induction furnace. Samples of gases on the inlet and exit sides of the furnace were analyzed and compared. Differences in the amounts of CO_2 in the inlet and exit gases indicated a

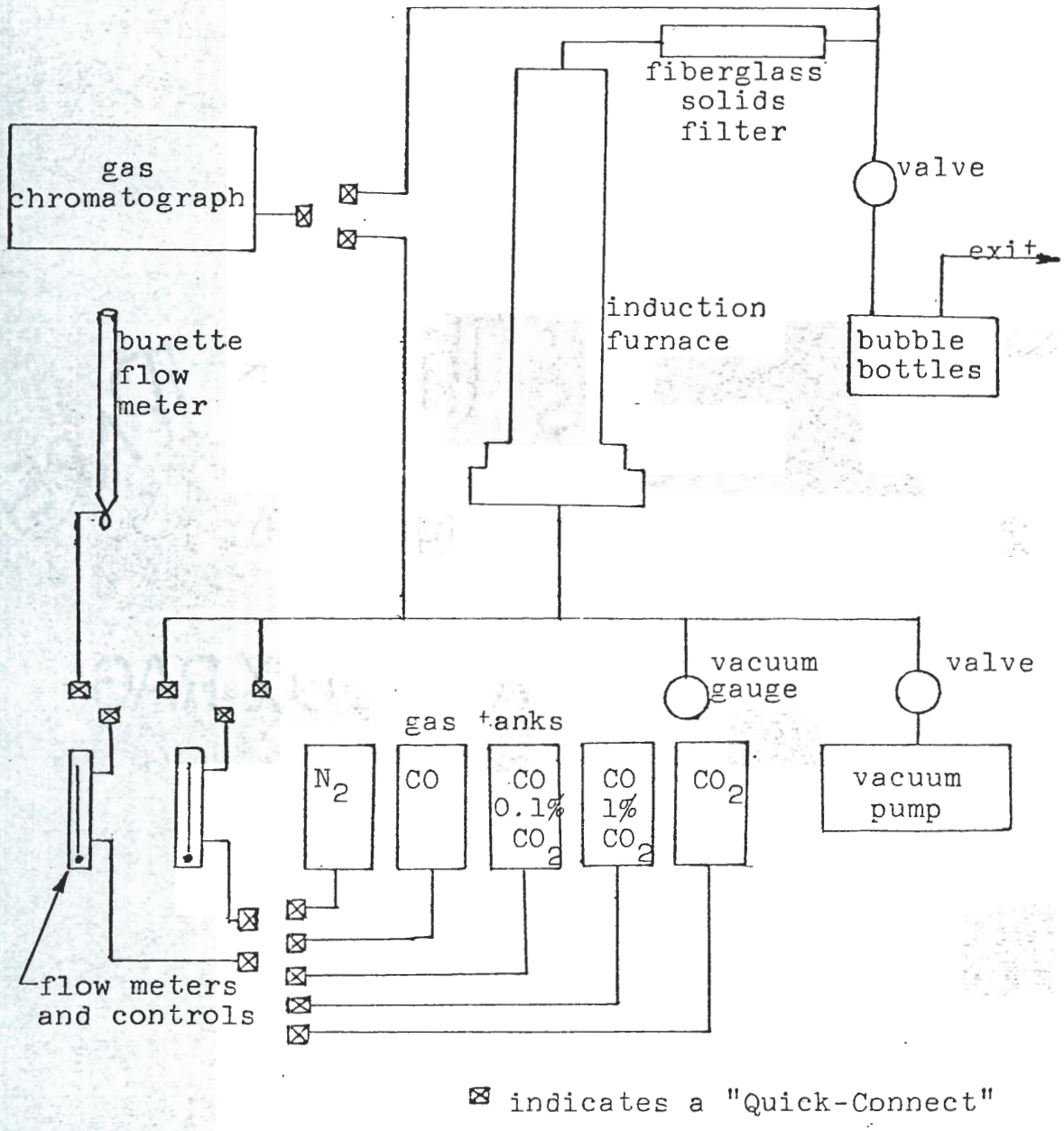

Figure 14. Schematic of gas control system.

reaction occurring between the ceria and the gas. Equilibrium in the sample was indicated by an identical analysis of the inlet and exit gas. The gas chromatograph was also used in conjunction with burette flow meter as a check on the CO/CO_2 analysis of the inlet gas mixture.

The gas chromatograph was a Carle Model 8500 containing a 6 foot long column of Porapak Q, 80-100 mesh, in a 1/8 inch diameter stainless steel tube. The chromatograph used a thermal conductivity detector, helium carrier gas at 5 ml/min, and a column and detector temperature of 50°C. A sample of CO/CO_2 gas could be easily analyzed in five minutes with this chromatograph. If necessary, other gases (N_2, O_2, H_2O, etc.), could be detected with a 4 foot column of Molecular Sieve 5A, 80-100 mesh by using "series/bypass" switching in the chromatograph.

The burette flow meter was used to accurately measure the flow rate of individual gases after they passed through the controlling valve and flow meter. The gas entered the burette and pushed a soap film bubble up the burette. A stop watch was used to measure the time it took for the bubble to indicate a flow of 100 milliliters. The flow rate was then calculated and the burette flow meter removed from the gas system. The analysis of a CO/CO_2 mixture was calculated from the individual CO and CO_2 flow rates. The burette flow meter was also used in the calibration of the gas chromatograph and

to control the helium carrier gas flow rate at 5.0 ml/min.

Temperature Calibration

The establishment of a known sample temperature for the solid CeO_{2-x} sample within the susceptor tube is described in this section. The outer surface of the susceptor tube was observed with an optical pyrometer to determine the "optical temperature." The temperature of the sample within the tube was higher than this external temperature even after the optical temperature was corrected for emissivity and absorption losses. The interior sample temperature was correlated with the optical temperature by determining the optical temperature at known interior temperatures using the melting points of several metals.

The calibration of the interior temperature of the iridium tube was accomplished by determination of the melting points of cobalt (1494°C), palladium (1554°C), and platinum (1772°C). The procedure consisted of placing a small piece of the metal within a cavity between two zirconia pellets. The pellets were placed within the iridium tube in the same position the ceria samples would occupy. The system was then heated to a certain optical temperature, held at temperature fifteen minutes, then cooled and disassembled. The metal was then examined to see if it had melted. A series of experiments above and below the melting points bracked the "optical temperature" corresponding to the melting points within a few

degrees. The melting points for cobalt, palladium and platinum respectively had the measured "optical temperatures" in the iridium tube of 1305°, 1365°, and 1510° ± 5°C.

The interior temperature of the smaller induction furnace using a molybdenum tube was calibrated in a similar fashion. Since this tube was used for higher temperatures, the calibration was done using platinum, 1772°C, and rhodium, 1963°C. The "optical temperatures" for these calibration points were 1480° ± 5°C and 1680° ± 5°C respectively.

The calibration points were used to draw graphs correlating the interior temperature with the observed optical temperature. The graph was assumed to be linear for two reasons: 1) the three points for the iridium furnace calibration had a maximum deviation of 8°C from a straight line, and 2) using a similar induction heated tungsten tube furnace Mordavid, et al.[33], found a linear correction in the optical temperature after using six calibration points.

The accuracy of the temperature control was estimated as ± 20°C. The error at the calibration points was only about ± 5°C but the possibility of additional errors was included in the ± 20°C spread. Other possible errors are variations in silica tube thicknesses changing the transmittance or drifts in the temperature during an experiment.

Procedure for Determining Solid CeO_{2-x} - Oxygen Pressure Equilibrium

This section describes the technique for determining the relationship between solid CeO_{2-x} and the equilibrium oxygen pressure for the temperature range 1477°C to 1808°C, with oxygen pressures 10^{-3} to 10^{-12} atmospheres. To obtain the low oxygen pressures mixtures of CO and CO_2 were used with the disassociation of CO_2 providing the oxygen. Ceria compositions between $CeO_{1.97}$ to $CeO_{1.65}$ were obtained under these conditions.

Certified grade cerium dioxide powder from Fisher, lot number 753750, was used to dry press sample wafers 1.9 cm diameter, about 0.5 cm thick. A sample wafer was placed between two larger ceria pellets and then positioned in the induction furnace, Figure 12. Care was taken to insure the same positioning of the sample in each experiment. The two thicker ceria pellets and thinness of the sample were utilized to minimize thermal gradients within the sample.

The induction furnace was evacuated to remove air and check the system for leaks. The furnace was then filled with N_2, and then heated, for about an hour, up to one of the selected temperatures of 1477°, 1587°, 1725°, or 1808°C. The N_2 flow was turned off and the furnace filled with a flowing predetermined mixture of CO and CO_2. Using the optical pyrometer, the temperature was adjusted to the exact desired value

and the input power to the furnace carefully noted. The CO/CO_2 gas mixture was analyzed using the gas chromatograph and by measuring each flow rate with the burette flow meter. The flow rate of the gas mixture ranged from 500 to 1000 ml/min which gave linear flow rates of 1.3 to 2.6 cm/sec around the sample. These flow rates were greater than the 0.9 cm/sec value recommended by Darken and Gurry[2] to eliminate thermal separation effects.

The temperature and gas composition were held constant while the composition of the CeO_{2-x} approached equilibrium. The furnace temperature was held constant by keeping the input power constant. This was necessary for, after extended times at the higher temperatures, vapor deposits on the silica tube sometimes prevented accurate optical temperature measurements. The ceria-gas reaction was monitored by periodically analyzing the exit gas composition with the gas chromatograph. Typically it required about four hours for the exit gas to match the inlet gas composition, indicating the solid CeO_{2-x} sample had reached equilibrium. The sample was held at temperature for one additional hour to assure equilibrium was obtained.

The system was purged with nitrogen to help retain the composition and then quenched, cooling to below dull red heat, <800°C, in 30 seconds.

After cooling to room temperature, the sample was removed from furnace and portions weighed in the platinum crucibles

within two minutes for analysis of the composition. The quickness of the weighing was necessary because CeO_{2-x} is pyrophoric, however, weight gains of the sample were not detected until 5 to 10 minutes after exposure to the air. When oxidation of the CeO_{2-x} did initiate, there was a rapid, significant weight gain, a change in color from a blue-black to white and considerably heating of the sample. If any slight oxidation of the CeO_{2-x} occurred before weighing the sample, it was not significant in the determination of the equilibrium composition.

Procedure for Determining Molten CeO_{2-x} Redox Equilibrium

This section describes the experimental technique for determining the redox equilibrium for ceria melted in controlled CO/CO_2 gas mixtures. The experimental method is named the "internal molten zone technique" because the molten oxide is contained within the interior of the sample pellet. This avoids the problems of contamination from contact and reaction with other container materials. The maximum temperature is limited by the liquidus temperature of the oxide being heated.

The internal molten zone technique employed the direct radio frequency (rf) induction heating of the ceria pellet. The high frequency, 3.6 megahertz, induction heating was necessary due to the low electrical conductivity typical of oxides. Heat was generated within the oxide pellet while the

outer skin layer of the pellet was kept slightly cooler by loss of heat through the high radiation of energy at temperatures above 1800°C. Careful control of the power input allowed enough heat to be generated to melt the interior of the pellet while surface remained solid.

The experimental procedure involved three steps: 1) preheating, 2) induction coupling and obtaining a stable molten zone, and 3) equilibrating the CeO_{2-x} composition in a fixed CO/CO_2 gas mixture. The preheating step was very simliar to the procedure in the solid ceria experiments except that a ceria pellet about 3 cm high was used instead of a thin sample wafer. The pellet was heated to 1600°C using the iridium susceptor tube around the pellet (very similar to Figure 12). Initial heating was in N_2 but at 1600°C the atmosphere was changed to an appropriate CO/CO_2 mixture. The pellet was held approximately an hour at these conditions to sinter, to densify, and to adjust the O/Ce ratio. If the composition were not adjusted to a value near the expected composition of the molten ceria, the pellet would explode upon melting due to a very rapid explusion of oxygen.

The second step in the melting procedure involved induction coupling to the ceria pellet and establishing a stable internal molten zone. The iridium preheat tube was quickly lowered out of the induction coil and the power increased. The ceria pellet was exposed to the electromagnetic

field and inductively coupled to the rf generator. At 1600°C the electrical conductivity of the oxide was high enough to allow rf induction heating within the pellet and the temperature was further increased up to the melting point. Since the heat was generated within the sample itself, the interior of the pellet was slightly hotter than the surface, which was cooled chiefly by thermal radiation losses. If the input power was carefully controlled, the interior of the pellet was melted while the surface remained solid containing the molten material. The melting of the interior was easily detected on the meters of the rf generator. The molten oxide had a much higher electrical conductivity than the solid. When the material melted the load to which the generator was inductively coupled rapidly changed and the grid current and plate voltage decreased. At this time, the power of the generator was quickly adjusted to prevent a runaway situation and melting of the solid surface layers. The power was decreased to a value that maintained a molten interior but did not cause further melting of the solid surface. The input power was then balanced with the losses of thermal energy creating a stable molten zone.

After the internal molten zone was stabilized, the CO/CO_2 mixture was adjusted to the ratio desired for the molten CeO_{2-x} redox equilibrium thus beginning the third step of the procedure. The pellet was held at constant temperature for

about four hours until the CeO_{2-x} composition equilibrated with the fixed CO/CO_2 gas mixture. Equilibrium was detected with the gas chromatograph by equal analyses of the inlet and exhaust gases. Conditions were maintained for an additional hour to assure equilibrium and then the sample was quenched in nitrogen.

The composition of the molten ceria was assumed to remain essentially constant during quenching. The pellet cooled from the molten state to below red heat (less than 800°C) in about 45 seconds. Since N_2 is not an actively reducing gas and there were no sources of oxygen in the system, the change in sample composition upon quenching was negligible. The cooled sample contained material of the same composition as the liquid and the unmelted solid surface layers. These two regions were very easily distinguished after crushing the sample pellet. The molten material had solidified into relatively large crystal grains and the solid maintained a very fine grain structure. The two materials were separated and the composition determined by weight gain upon oxidation to $CeO_{2.0}$. The composition of the molten oxide was determined for every experiment, whereas the composition of the solid oxide was measured in only a few experiments.

Procedure for Determination of Liquidus Temperatures for CeO_{2-x}

Since there was no means of measuring the temperature of the molten ceria with the internal molten zone technique, another method was necessary to determine the liquidus temperature. Small samples of ceria were heated to various temperatures in a known gas mixture and examined to determine at what temperature the melting first occurred. The smaller diameter induction furnace, Figure 13, capable of achieving temperatures above 2000°C, was used because the larger furnace could not be consistently heated above 1830°C.

The small induction furnace used a molybdenum susceptor which reacted with the CO/CO_2 atmosphere if greater than 10% CO_2 was present thus limiting the oxygen pressure range. A small diameter iridium tube would circumvent this problem but was not available for these experiments.

The procedure was to place a piece of ceria about 2 millimeters in diameter on the zirconia support shown in Figure 13. The furnace was evacuated and then filled with a known CO/CO_2 mixture. The furnace was then quickly heated, reaching the experimental temperature in one to two minutes. The gas chromatograph was used to monitor the exit gas to determine when the ceria had equilibrated with the gas mixture. Since the ceria sample was small, equilibrium was typically reached in 10 to 15 minutes. The sample was quenched and removed for examination. Samples were heated to successively

higher temperatures until evidence of melting was observed, and the melting temperature for that gas mixture determined. The series of experiments was then repeated using a different gas mixture.

To detect melting of the material, the ceria sample was broken in half exposing its interior. The pieces were placed in the scanning electron microscope, SEM, and examined at high magnifications. Unmelted samples were distinguised by a blocky grain structure with sharply defined edges. Melted samples had smooth flowing features without evidence of the previous grains.

Control of Oxygen Pressures

The low oxygen potentials or oxygen partial pressures in the furnace were established by controlling the CO/CO_2 ratio in the gas mixture. Well established thermodynamic techniques[3,4] based on the disassociation of CO_2, equation 1, were used to calculate the oxygen pressure.

$$2CO_2 \rightarrow 2CO + O_2 \qquad (1)$$

The free energy of the reaction, ΔF, at the desired temperature was calculated from tables of thermodynamic data[38]. The oxygen pressure was related to the free energy, temperature, and CO/CO_2 ratio by equations 2-4.

$$\Delta F = -RT \ln K \tag{2}$$

$$\Delta F = -RT \ln \left[\frac{(Pco)^2 (Po_2)}{(Pco_2)^2}\right] \tag{3}$$

$$Po_2 = \left(\frac{Pco_2}{Pco}\right)^2 \exp\left(\frac{\Delta F}{-RT}\right) \tag{4}$$

where: T = absolute temperature

K = equilibrium constant for reaction (1)

R = gas constant

Po_2 = partial pressure of O_2

Pco_2 = partial pressure of CO_2

Pco = partial pressure of CO

The total pressure in the system was assumed to be one atmosphere and the partial pressures of CO and CO_2 were assumed equal to their volume percents in the gas mixture. Oxygen pressures in the range 10^{-3} to 10^{-12} atmospheres were attained by this technique.

The utilization of CO/CO_2 gas mixtures was limited to values yielding oxygen pressures less than about 10^{-3} atmospheres. At higher oxygen pressures the CO/CO_2 ratio in the inlet or exhaust gas did not describe the conditions at the elevated temperature. The disassociation of CO_2 was high enough to significantly alter the CO/CO_2 ratio making the calculations meaningless.

The lower range of oxygen pressure was limited by the occurrence of a side reaction in the gas. Under certain conditions carbon mcnoxide decomposed by Equation 5.

$$2CO \rightarrow CO_2 + C \qquad (5)$$

Thermodynamic calculations indicated the reaction should occur at room temperature but the kinetics of the reaction are very slow and usually prevent significant decomposition of CO. The kinetics require high temperatures and a catalyic surface. At temperatures above 1500°C the reaction is not thermodynamically favorable in most CO/CO_2 mixtures. The reaction occurred in the cooler regions of the furnace (estimated at 300-700°C) as the gas was being heated and the deposition of solid carbon was a clear indication of the reaction. However, the rate of the reaction was so slow that it usually did not significantly alter the CO/CO_2 ratio. The inlet and exhaust gases usually would come to equilibrium within the resulation of the gas chromatograph even when deposited carbon was observed in portions of the furnace. In general, equivalent inlet and exhaust gas ratios were established if the CO_2 content was 1% or greater. An inlet gas of 0.1% CO_2 was converted to an exhaust gas containing 0.2 to 0.3% CO_2. This indicated that reaction 5 would alter the CO_2 content by a few tenths of a percent which became significant only when the CO_2 content was less than 1%. Thus minimum oxygen pressure obtainable

was limited by the inability to utilize gas mixtures containing less than 1% CO_2.

The ceria sample was not contaminated by carbon deposition from reaction 5. During equilibration, the ceria samples were at 1500° or higher, much above the temperature at which this reaction is thermodynamically favorable. The reaction could not occur while the sample was being preheated up to the high temperature because nitrogen was used during preheating instead of the CO/CO_2 mixtures.

The accuracy of the calculated oxygen pressure depended upon the accuracy of the thermodynamic data, the experimental temperature, and the composition of the CO/CO_2 gas mixture. The largest possible error in the oxygen pressure was calculated by combining the worst errors in the temperature and gas composition. Error in the temperature was $\pm$ 20°C. Error in the gas composition was based upon the error in the individual flow rates which was usually a few percent. Using the worst possible combination of errors, the highest and lowest possible oxygen pressures were calculated along with the "correct" oxygen pressure for each experiment. This information is shown in Appendix A.

Determination of CeO_{2-x} Composition

The CeO_{2-x} composition or the O/Ce ratio of the ceria sample after quenching was determined by the weight change

upon conversion to a known reference composition $CeO_{2.000}$. Substoichiometric ceria, CeO_{2-x} converts to stoichiometric $CeO_{2.000}$ when heated in air at 800°C as shown in equation 6. If the initial and final weights of a ceria sample were known, the composition of value of x in the initial CeO_{2-x} was easily calculated.

$$CeO_{2-x} + x/2\ O_2 \rightarrow CeO_{2.0} \tag{6}$$

The experimental procedure was to remove the CeO_{2-x} sample from the furnace system after it had cooled overnight in N_2. The sample was broken and portions placed in two pre-weighed platinum crucibles. The platinum and ceria were then weighed together and placed in a small furnace. The furnace which had openings to allow sufficient air ventilation was heated overnight at 800°C. After cooling the platinum and ceria were reweighed. Using the weights of the platinum crucibles (PT), the platinum and CeO_{2-x} (CX) and the platinum and $CeO_{2.0}$ (CD), the value of x was calculated using equation 7 and the PDP-8 computer.

$$x = 10.7578 * \frac{(CD - CX)}{(CD - PT)} \tag{7}$$

The numerical factor in equation 7 is the molecular weight of $CeO_{2.0}$ divided by the atomic weight of oxygen.

The error in the calculated ceria composition depended upon the accuracy of the three weighings, estimated as $\pm$ 0.0002

grams. The largest possible error in the composition was calculated by combining the errors in the weighings to give the greatest deviation from the "correct" value. This error was calculated and printed as a "$\pm$" value following the "correct" composition as shown on the computer printouts in Appendix A.

CHAPTER IV

RESULTS

This chapter lists the results from the redox experiments and melting point determinations for CeO_{2-x}. The chapter is divided into sections covering the solid CeO_{2-x} - oxygen pressure equilibrium, the internal molten zone experiments, and the melting point determinations. The experimental data used to calculate the results are given along with error calculations in the computer printouts in Appendix A. The oxygen pressures were calculated using thermodynamic data from the JANAF tables[38].

Solid CeO_{2-x} - Oxygen Pressure Equilibrium Results

The results of equilibrating solid CeO_{2-x} with atmospheres of selected oxygen pressures at 1477°, 1587°, 1725°, and 1808°C are given in Tables 2, 3, 4 and 5 respectively. The tables list the percent CO_2 in the CO/CO_2 mixtures, the calculated oxygen pressures, and the two measured solid compositions for each experiment. The oxygen pressure and compositions are plotted in Figure 15 with straight isotherms from a linear regression calculation.

Molten CeO_{2-x} - Redox Equilibrium Results

The results of the internal molten zone experiments are

Table 2. Oxygen Pressure-Composition Relationship for CeO_{2-x} at 1477°C.

Experiment Number	Percent CO_2	-Log P_{O_2}	Composition n in CeO_n	
18	24.2	8.84	1.8148	1.8175
19	31.0	8.54	1.8332	1.8315
25	39.3	8.01	1.8463	1.8457
26	39.3	8.23	1.8455	1.8416
28	92.1	5.71	1.9446	1.9401
29	80.5	6.61	1.8991	1.9010
30	6.0	10.23	1.7874	1.7823
31	6.0	10.23	1.7778	1.7778
32	10.1	9.75	1.7927	1.7971
33	6.1	10.22	1.7603	1.7612
34	10.1	9.74	1.7765	1.7770
35	6.8	10.12	1.7680	1.7581
36	4.8	10.45	1.7622	1.7586
37	1.1	11.76	1.7240	1.7223
39	2.4	11.07	1.7382	1.7369
40	0.2	13.24	1.6843	
42	38.3	8.26	1.8481	
43	48.4	7.90	1.8660	1.8618
44	95.8	5.13	1.9548	1.9542
45	1.0	11.84	1.7183	1.7228
57	1.0	11.83	1.7202	1.7247
58	96.4	5.00	1.9539	1.9512
64	96.5	4.96	1.9574	
78	59.0	7.53	1.8719	1.8726
79	84.4	6.38	1.9195	
80	95.8	5.13	1.9583	

Table 3. Oxygen Pressure-Composition Relationship for CeO_{2-x} at 1587°C.

Experiment Number	Percent CO_2	-Log P_{O_2}	Composition n in CeO_n	
60	1.0	10.85	1.6939	1.6996
61	86.3	5.26	1.9093	1.9076
62	48.3	6.92	1.8541	1.8574
63	7.9	9.00	1.7730	1.7811
72	1.0	10.85	1.7054	1.6990
73	4.5	9.52	1.7554	1.7607
74	95.9	4.12	1.9473	
81	41.1	7.18	1.8351	1.8375
82	28.8	7.65	1.8126	1.8045
83	27.8	7.69	1.8169	1.8162
84	17.0	8.24	1.8018	1.8069
85	71.8	6.05	1.8727	1.8769
86	2.2	10.16	1.7277	1.7178
87	0.2	12.26	1.6727	1.6737
88	94.2	4.44	1.9386	1.9389

Table 4. Oxygen Pressure-Composition Relationship for CeO_{2-x} at 1725°C.

Experiment Number	Percent CO_2	-Log P_{O_2}	Composition n in CeO_n	
89	90.4	3.84	1.8988	1.8973
90	80.9	4.53	1.8707	1.8765
92	28.8	6.57	1.7889	1.7960
93	26.2	6.68	1.7894	1.7961
94	39.3	6.16	1.8172	1.8182
95	59.4	5.45	1.8429	
96	0.3	10.83	1.6518	1.6538
104	3.2	8.75	1.7094	1.7105
105	10.5	7.65	1.7582	1.7586
106	4.5	8.44	1.7276	1.7298
107	1.0	9.77	1.6761	1.6847

Table 5. Oxygen Pressure-Composition Relationship for CeO_{2-x} at 1808°C.

Experiment Number	Percent CO_2	-Log P_{O_2}	Composition n in CeO_n	
97	80.1	4.00	1.8576	1.8559
98	87.8	3.49	1.8682	1.8735
99	47.3	5.30	1.8120	1.8109
100	11.8	6.95	1.7548	1.7552
103	3.2	8.17	1.7092	1.7101
108	1.0	9.19	1.6616	1.6525
109	29.2	5.97	1.7823	1.7867

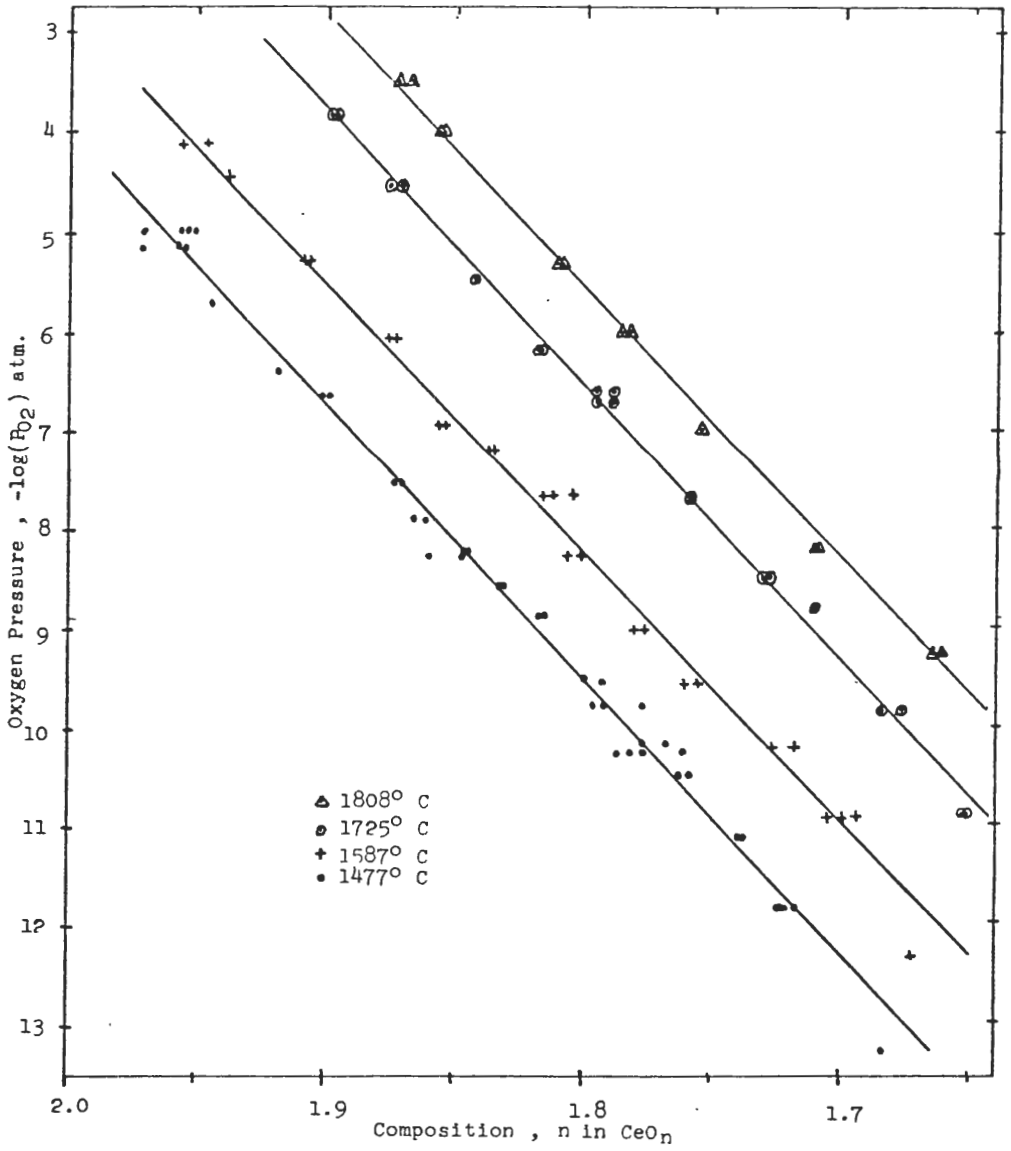

Figure 15. Results for Solid CeO_{2-x} - Oxygen Pressure Equilibrium.

listed in Table 6. The percent CO_2 in the CO/CO_2 gas mixture and the measured oxide compositions are given. The composition of the molten CeO_{2-x} was measured in all experiments but the solid CeO_{2-x} was measured in only three experiments. Two determinations of the molten CeO_{2-x} compositions were made for the experiments in which the solid compositions was not measured. Oxygen pressures for the gas mixtures are not given here because the necessary temperatures were not measured in the experiments.

Table 6. Molten CeO_{2-x} Redox Equilibrium Results

Experiment Number	Percent CO_2	Composition Liquid	n in CeO_n Solid
46	1.0	1.5968	1.6601
47	1.0	1.6000	
110	5.3	1.6416	1.7360
111	10.0	1.6631	
		1.6745	
112	15.6	1.6926	
115	29.5	1.7124	
		1.7164	
116	36.7	1.7294	1.8225
117	60.9	1.7552	
		1.7657	

Liquidus Temperature Determinations

The liquidus temperatures of CeO_{2-x} in equilibrium with three different CO/CO_2 gas mixtures were determined in the small induction furnace. The percent CO_2, the liquidus temperature, and the calculated oxygen pressure are listed in Table 7.

Table 7. Melting Temperatures for CeO_{2-x} in Equilibrium with Various Oxygen Pressures.

Percent CO_2	Melting Point °C	Oxygen Pressure -Log P_{O_2}
1.0	1850	8.9
5.3	1930	6.9
10.0	1970	6.1

CHAPTER V

DISCUSSION OF RESULTS

The experimental results are analyzed in this chapter. First, the equilibrium between solid CeO_{2-x} and oxygen pressure is discussed with a comparison to the literature information at lower temperatures. Then the internal molten zone experiments are used to establish the composition changes in molten CeO_{2-x} as a function of oxygen pressure. The derivation of the liquidus line is explained and the resulting phase diagram presented. The final section reviews the utilization of the internal molten zone technique to determine redox equilibria in molten refractory oxides that possess stoichiometric changes.

Solid CeO_{2-x} - Oxygen Pressure Equilibrium

The redox equilibrium in solid CeO_{2-x} is presented in Figure 15 as isotherms at 1477°, 1587°, 1725°, and 1808°C. To compare these results with equilibrium at lower temperature the oxygen pressure is shown as isobars in Figure 16. The isobars below 1500°C were from results of Panlener[24] which were replotted in Figure 21 of Appendix C for easier analysis.

Comparison of the results of this study and those of Panlener show good agreement at low oxygen pressures and a

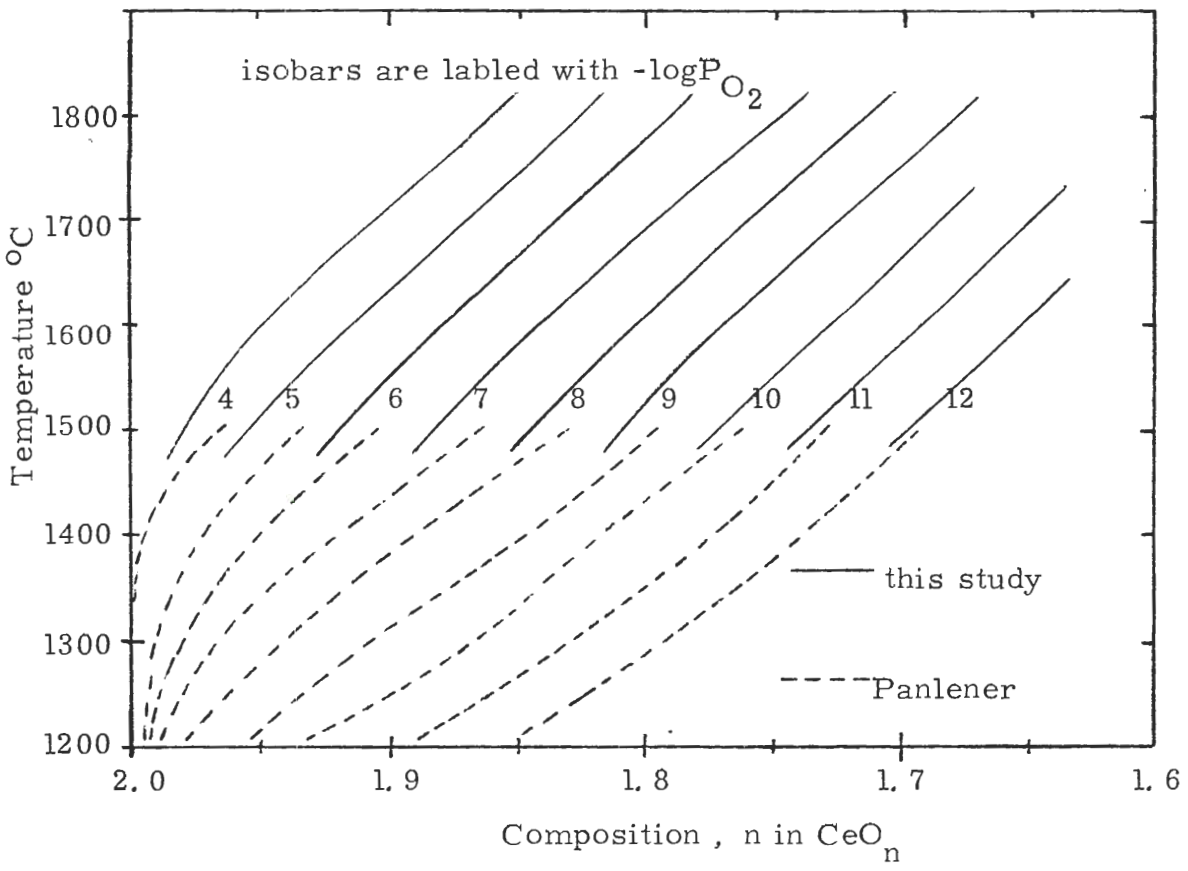

Figure 16. Solid CeO_{2-x} - Oxygen Pressure Equilibrium from this Study Compared with Lower Temperature Equilibrium Determined by Panlener.[24,25]

small disagreement at higher oxygen pressures. At oxygen pressures of 10^{-10} to 10^{-12} atm., the results agree within the reported experimental errors. At pressures of 10^{-4} or 10^{-5} atm. the disagreement is the most extreme. The difference expressed in the terms of ceria composition is a variation of 0.1 to 0.2 in the value of n in CeO_n. In both studies the compositions were determined by weight gains upon oxidation of CeO_{2-x} to CeO_2. The region of disagreement is at ceria compositions which had very small weight gains upon oxidation. Any error in measuring this weight gain resulted in significant errors in the composition. Panlener[24] was very skeptical of his own results in this composition region because of possible errors in his method of weighing at high temperatures and uncertainty of complete oxidation to $CeO_{2.00}$. The present investigation avoided the difficulties that Panlener encountered by doing all weighings at room temperature and by oxidation at conditions well known to give stoichiometric CeO_2.

A continous single phase region from CeO_2 to $CeO_{1.65}$ was indicated by the slope of the isotherms in Figure 15. An isotherm would have to be horizontal (constant pressure with varying bulk composition) to indicate a two phase region. The results of Panlener, Appendix C, also showed linear isotherms with similar slopes at temperatures above 1000°C. At lower temperatures, 700-800°C, the slopes of Panlener's isotherms decrease to a almost horizontal region near $CeO_{1.9}$. This

decrease in slope is due to the influence of the two phase region at slightly lower temperatures. At elevated temperatures, neither the isotherms of this investigation, Figure 15, nor of Panlener's study, Appendix C, show any similar decrease in slope. The single phase region extending from CeO_2 to $CeO_{1.65}$ is consistent with the results reported by Brauer and Gingerich[19], Kuznetsov, et al.[20], and Panlener[24,25]. But Bevan and Kordis[21] reported a two phase region in the range $CeO_{1.72}$ - $CeO_{1.70}$ at temperatures above 1023°C. In order for this two phase region not to conflict with other results, it must close between 1023° and 1300°C to allow for the single phase region. A similar relationship is well established in the region CeO_2 - $CeO_{1.8}$ in which the two phase region closes at about 685°C to form the single phase region at higher temperatures.

Molten CeO_{2-x} - Redox Equilibrium

In this section the results of the internal molten zone technique are analyzed to determine the usefullness of this method in the investigating redox equilibrium in molten CeO_{2-x}.

When discussing the internal molten zone technique, the conditions in the pellet can not be described with traditional equilibrium concepts. The solid exterior surface of the sample exposed to the CO/CO_2 gas mixture was typically

between 1800° and 2000°C. The molten interior of the CeO_{2-x} pellet was at the liquidus temperature between about 1850 and 2400°C, depending upon the composition. The obvious inherent difficulty of the technique was selecting the proper temperature for use in the calculation of the oxygen potential of the CO/CO_2 gas mixture. In the internal molten zone technique, equilibrium was assumed between solid oxide, liquid oxide, and oxygen in the gas phase. The equilibrium conditions are thus given on the phase diagram at the intersection of the pertinent oxygen isobar with the solidus and liquidus lines. The liquid compositions listed in Table 6 represent the equilibrium liquidus composition for each experimental condition.

In a similar determination of the redox equilibrium in molten $UO_{2\pm x}$, Chapman, et al.[5], made a strong case for using the temperature of the molten urania as the conditions establishing the oxygen potential in the gas mixture. The temperature and composition of the molten $UO_{2\pm x}$ was believed to represent conditions on the liquidus line since there was equilibrium between solid and liquid phases. In the following sections evidence is presented that the temperature of the molten CeO_{2-x} also determined the oxygen pressure in the CO/CO_2 mixture.

Analysis of the redox equilibrium data, presented in Table 6, for molten CeO_{2-x} was complicated by the lack of any

literature values for the liquidus and/or solidus temperatures in the CeO_2-Ce_2O_3 system and the nature of the internal molten zone technique prevented direct measurements of the liquid temperature. For the first step of the analysis, oxygen pressures were calculated for a range of temperatures for each gas mixture listed in Table 6. A portion of this information is shown in Figure 17. Calculated oxygen pressures, -log P_{O_2} atm., are given at their corresponding temperatures along vertical lines representing the liquidus composition determined in the stated gas mixture. Sloping isobars at lower temperatures represent solid CeO_{2-x}-oxygen pressure equilibrium. The goal of the analysis was to extend the isobars for solid CeO_{2-x} upward to meet the liquidus compositions (vertical lines in Figure 17) at the appropriate temperature. However this cannot be a simple extrapolation of the sloping isobars because a horizontal (isothermal) portion must be included as the isobar crosses the two phase region between the solidus and liquidus lines. To determine the location of the isothermal portion of a particular isobar, a measurement of the melting point of CeO_{2-x} in that oxygen pressure was necessary. The following section, "Determination of Liquidus Temperatures for CeO_{2-x}" describes these measurements.

An effort was also made to establish the composition of the solid in equilibrium with the molten ceria by analysis of the unmelted skin adjacent to the molten zone. Selected

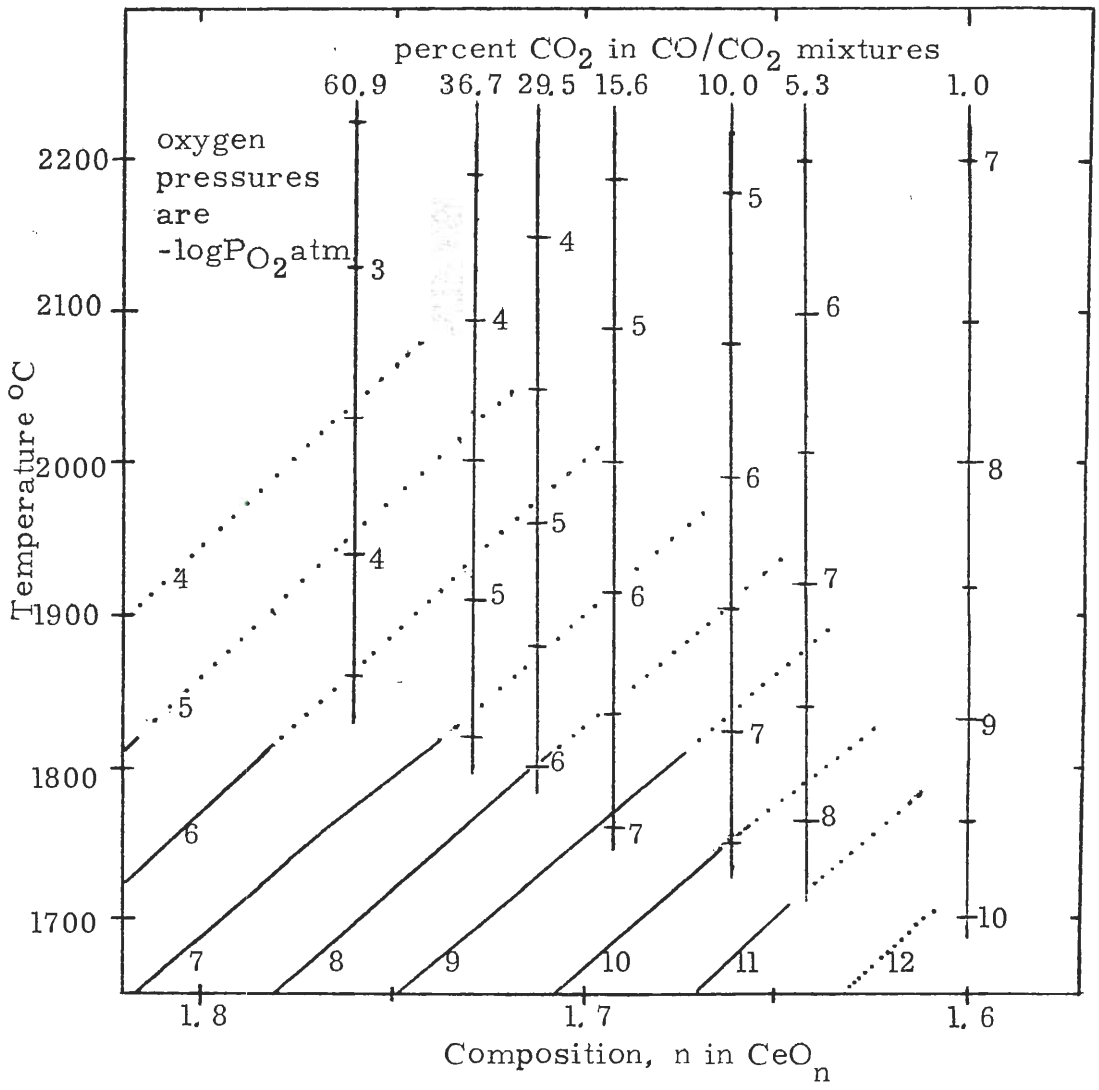

Figure 17. Liquidus Compositions from Internal Molten Zone Experiments Compared with Oxygen Isobars for Solid CeO_{2-x}. Vertical lines represent liquidus compositions determined in the stated gas mixtures with oxygen pressures calculated for a range of temperatures.

solidus composition values are listed in Table 6, however this data was inconsistent and probably does not represent equilibrium conditions for the solidus because of the large thermal gradients in the solid. Therefore, the solid compositions in Table 6 cannot be used in the analysis of the redox equilibrium.

Determination of Liquidus Temperatures for CeO_{2-x}

To determine the location of the liquidus and solidus curves on the CeO_2-Ce_2O_3 phase diagram it was necessary to measure the melting points for various ceria compositions. The smaller induction furnace, Figure 13, was necessary equipment because the larger furnace would not heat to the desired temperatures. Melting points for three ceria compositions were measured using the same CO/CO_2 mixtures (10%, 5.3%, and 1% CO_2) that had been used in previous internal molten zone experiments. The use of these specific gas mixtures allowed the measurement of temperatures that correlated with the determined liquidus compositions. It was not necessary to know the solid ceria composition since the results were solidus or liquidus temperatures corresponding to particular gas mixtures. Oxygen pressures were calculated for the experiments from the CO/CO_2 mixture and the measured temperature.

The analysis of the technique for determining the melting points depended upon two major considerations. First was the

question of whether or not there was equilibrium between the gas mixture and the ceria. The second concerned the ability to detect the initial melting of the ceria.

Evidence of equilibrium between the gas and the solid ceria was obtained from the gas chromatograph. Analysis of inlet and exit gas compositions during the initial minutes of an experiment indicated higher CO_2 concentrations in the exit gas. The amount of excess CO_2 decreased until after 10 to 15 minutes at constant temperature the inlet and exit concentrations were equal and remained constant. This was expected because the ceria sample initially contained more oxygen than the final composition. The ceria was being reduced by the gas, giving off oxygen which reacted to form excess CO_2. When the reaction ceased, and equilibrium was established between the gas and solid ceria, the inlet and exit gas compositions were identical.

The melting characteristics of a solid solution should be reviewed to understand the question concerning the ability to detect the initial melting (solidus temperature) of the ceria samples. The melting behavior of a solid solution depends partly on the experimental conditions. Two techniques will be considered. First, a sample sealed in an inert capsule to prevent any bulk composition change in the sample will melt over a temperature range. Melting initiates at the solidus temperature for the composition and is complete

at the liquidus temperature. The difference between these temperatures might be fifty to a hundred degrees in some systems. To detect the solidus temperature in this technique requires a method for detecting the formation of the initial infinitesimal quantity of liquid. The second technique involves a sample in equilibrium with a gas of constant composition. In this method, the bulk sample composition must change in order to remain in equilibrium with the gas phase. If equilibrium conditions could be maintained in this technique, a solid solution would melt completely at a fixed temperature instead of over a temperature range. Consider an oxide solid solution in equilibrium with a flowing CO/CO_2 gas mixture. As the oxide is heated, the solid composition changes to remain in equilibrium with the oxygen partial pressure produced by the gas mixture. When the solidus temperature is reached, the system contains a fixed oxygen pressure, solid oxide of the solidus composition, and liquid oxide of the liquidus composition. If equilibrium conditions were maintained between the oxide and gas, the entire melting would take place isothermally. This requires a change in the bulk sample composition from the solidus to the liquidus composition. The liquidus and solidus temperatures are identical if equilibrium is maintained with a set gas composition.

The technique for determining the melting points in this study was best described by the second technique above. The

method of heating the sample in the flowing gas mixture and holding at a particular temperature allowed equilibrium to be established between the ceria and gas. Samples were heated in the same gas mixture to temperatures increasing in steps of about 10° to 20°C. Below the melting point the samples did not show evidence of liquid formation upon examination in the scanning electron microscope. Sample heated above the melting point has evidence of complete melting. The melting point for each gas mixture was determined with an accuracy of about $\pm$ 20°C by this technique.

The measured liquidus temperatures for CO/CO_2 gas mixtures containing 1.0%, 5.3%, and 10.0% CO_2 are listed in Table 7 along with calculated oxygen pressures. Attempts to determine liquidus temperatures in gas mixtures of higher CO_2 content failed due to oxidation of the molybdenum tube.

Determination of the Liquidus and Solidus Lines

The procedure used for the determination of the liquidus and solidus curves is described in this section. Liquidus compositions for specific gas mixtures are listed in Table 6. Liquidus temperatures and oxygen pressures for three of these gas mixtures are given in Table 7. The three known liquidus compositions and temperatures were plotted in Figure 18. Isobars of these temperatures were extended from the composition points to the left across the two phase (liquid and solid)

region. The corresponding isobars that had been determined for the solid phase at lower temperatures were extrapolated upward to meet the horizontal isobars. The intersection of these lines determined the solidus composition for that specific oxygen pressure. The portions of the liquidus and solidus lines determined by this procedure are shown as solid lines in Figure 18.

The initial approximation of the remaining portions of the liquidus line was drawn by extending the determined portions of the lines to the melting points of CeO_2, 2480°C, and Ce_2O_3, 1692°C. The remaining liquidus compositions were assigned temperatures based upon this line. Oxygen pressures were calculated from the CO/CO_2 gas mixture and these temperatures. Solidus points were then determined by the intersection of the horizontal isobars with the corresponding extrapolated oxygen pressures for CeO_{2-x}. When discrepancies occurred slight adjustments were made to the liquidus and solidus temperature until smooth curves, consistent with the oxygen isobars, were obtained. Table 8 lists the measured and derived temperatures, compositions, and oxygen pressures for the specific CO/CO_2 gas mixtures. Figure 19 shows this experimental data in a composite diagram along with the solid CeO_{2-x} - oxygen pressure equilibrium at lower temperatures.

The phase diagram, for the CeO_2 - Ce_2O_3 system is presented as Figure 20. This diagram shows equilibrium oxygen

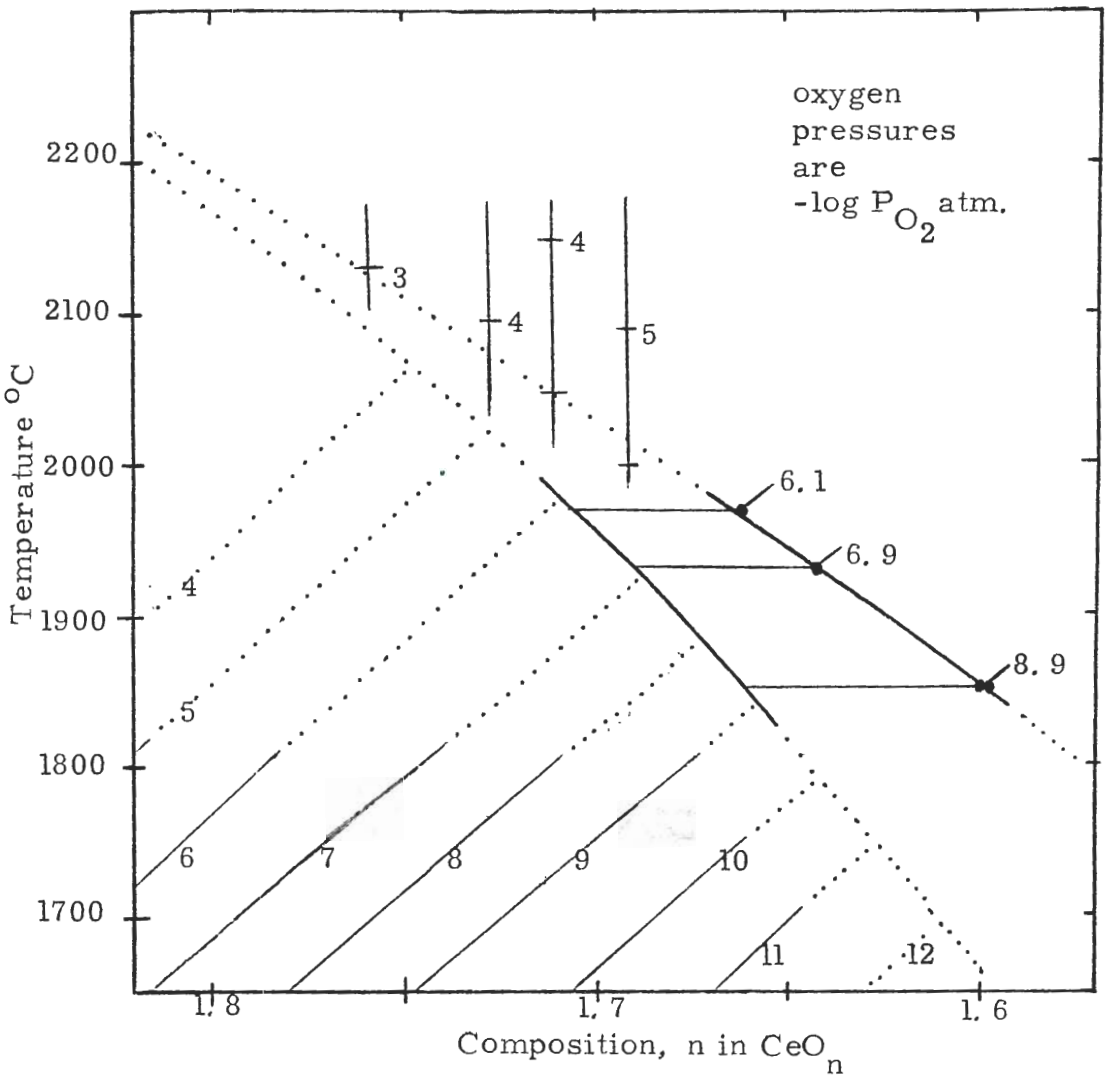

Figure 18. Derivation of Liquidus and Solidus Curves with Measured Temperatures for Three Liquidus Compositions.

Table 8. Measured and Derived Data for Liquidus and Solidus Curves for Specific Gas Mixtures.

Percent CO_2	Composition, n in CeO_n Derived Solidus	Measured Liquidus	Temperature, °C Derived	Measured	Oxygen Pressure -Log P_{O_2}
1.0	1.66	1.60		1850	8.9
5.3	1.69	1.64		1930	6.9
10.0	1.71	1.66		1970	6.1
15.6	1.72	1.69	2010		5.4
29.5	1.74	1.71	2050		4.5
36.7	1.75	1.73	2070		4.1
60.9	1.78	1.76	2030		3.0

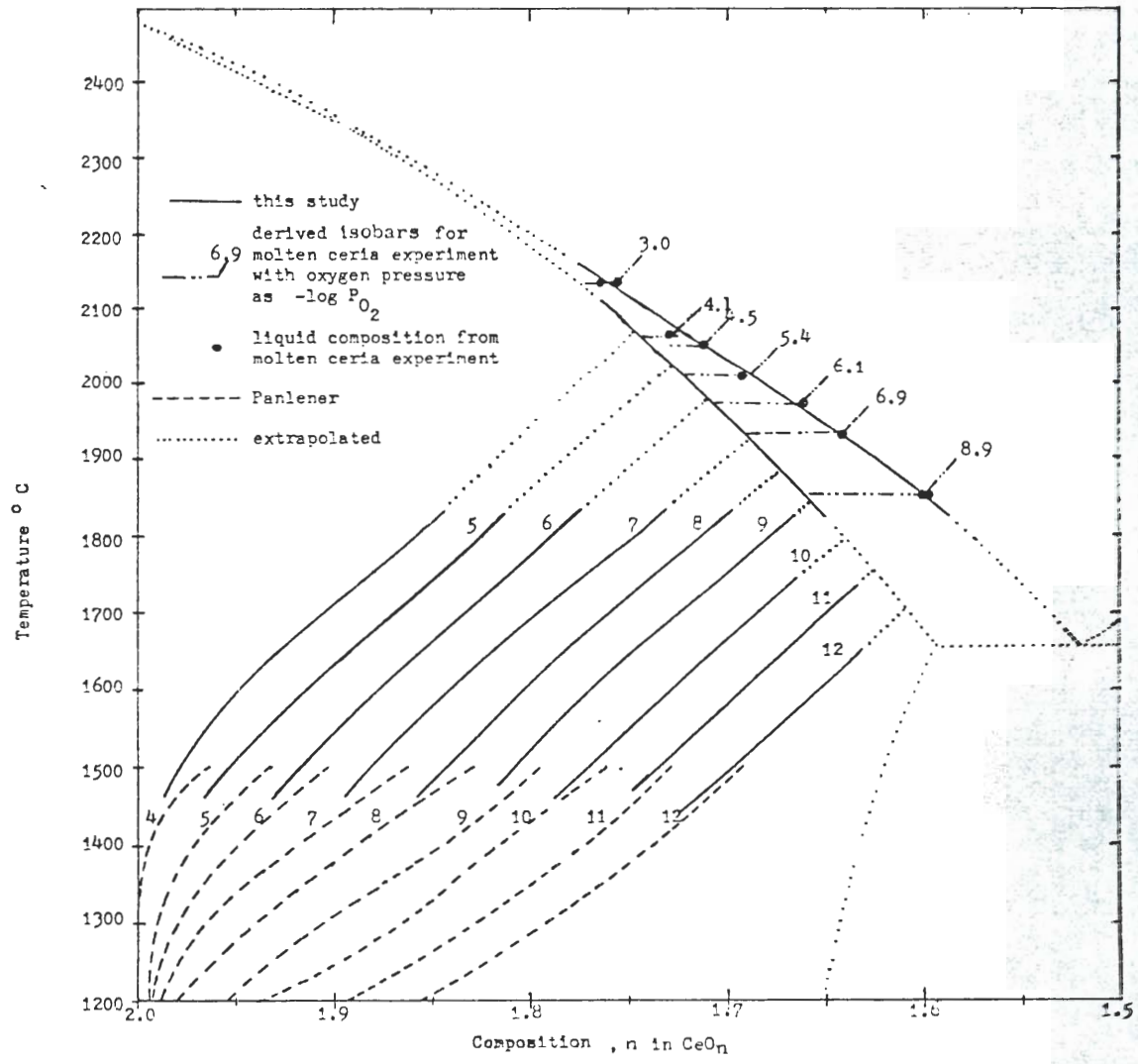

Figure 19. Composite Diagram for CeO_2-Ce_2O_3 System Showing Results of this Study and Data from Panlener[24,25].

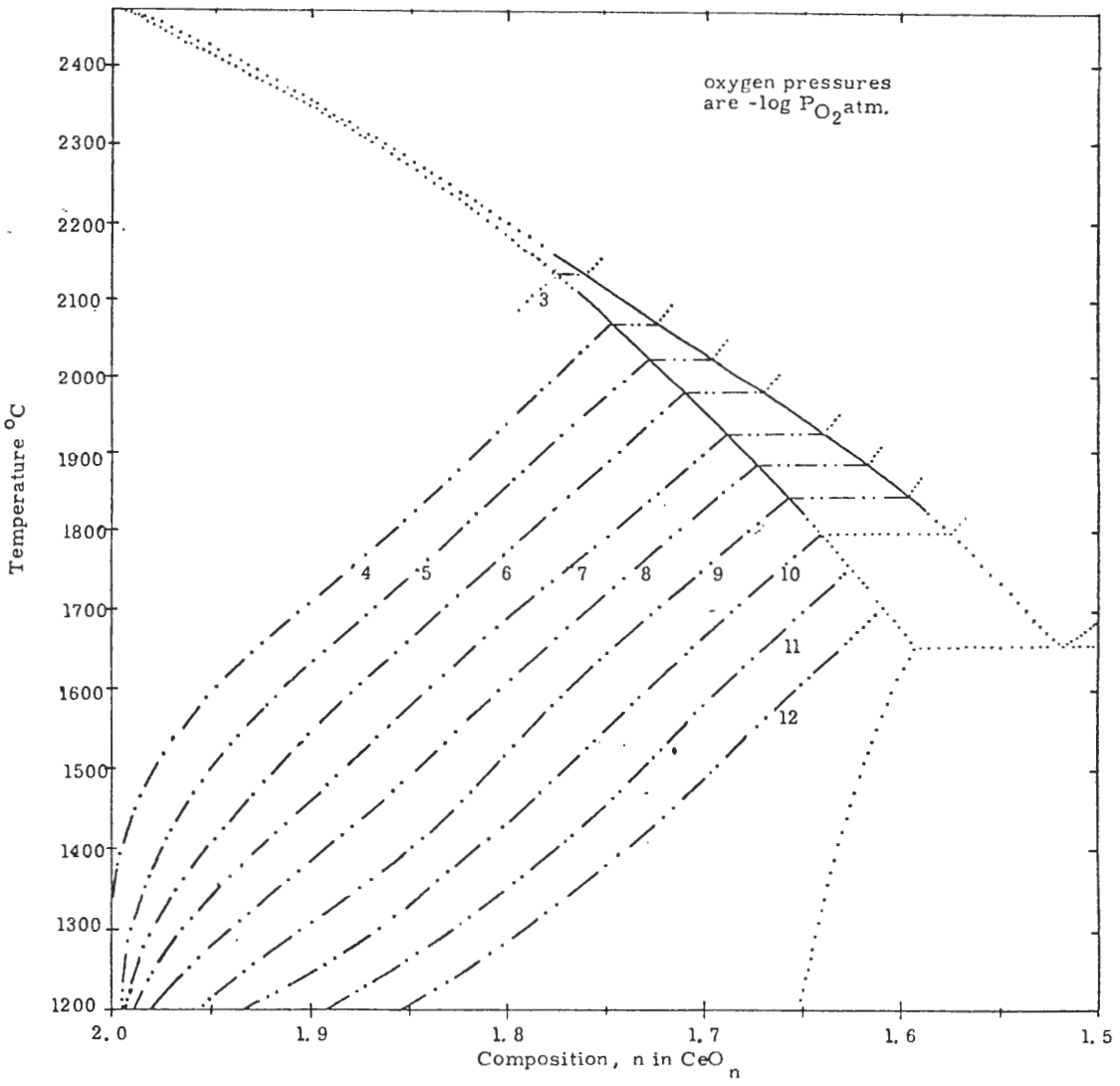

Figure 20. Phase Diagram for CeO_2-Ce_2O_3 System above 1200°C with Isobars Showing Oxygen Pressure Equilibrium.

pressures as isobars extending from 1200°C to the liquidus line.

Evaluation of the Internal Molten Zone Technique for Determination of Redox Equilibrium

In the preceding sections of this work it has been possible to assemble a phase diagram for CeO_{2-x} at temperatures up to and including the liquidus curve for this material. The stoichiometric changes observed in solid CeO_{2-x} were collected using conventional isothermal equilibration of ceria samples in controlled oxygen pressures. However, the unique and potentially troublesome information generated in this work was obtained using the internal molten zone technique. The areas of uncertainty in this approach include the uniformity of the temperature within the molten liquid itself and the large temperature gradients existing across the solid skin required to maintain and contain the molten material. In order to utilize molten zone data it was necessary to postulate that the temperature of the molten pool and solid skin adjacent to the pool were essentially at the liquidus temperature of the equilibrium system for CeO_{2-x} and that this temperature controlled the oxygen pressure of the CO/CO_2 gas mixtures used. The following discussion is an attempt to justify these statements.

During the induction heating of the CeO_{2-x} samples, the presence of the heating caused stirring in the molten material.

These currents certainly acted as a source of motion to minimize temperature gradients in the liquid. In addition, experimental evidence was also collected to support the lack of temperature gradients in the liquid. In experiments using the same CO/CO_2 gas mixtures but varying the input power to the sample an identical liquid compositions, within experimental error, was measured. The higher input power did not serve to increase the temperature of the liquid but merely increased the size of the molten pool. Apparently any effort to increase the temperature of the molten pool was practically impossible since the liquid was in contact with the solid CeO_{2-x} skin. This behavior was used advantageously to obtain large samples for the measurement of the liquid composition.

While enough material was readily available for determining the liquid composition, the composition of the thin solid layer of material containing the molten zone was difficult to measure. The steep temperature gradient in the solid skin was accompanied by a composition gradient and it was impossible to select areas small enough to obtain reproducible composition values. Even attempts to obtain the solid sample from the region directly below the center of the molten zone gave inconsistent results. Only in the experiments using the 1% CO_2 mixture that resulted in samples with the lowest internal temperature was the measured solid composition near the solidus composition shown in Figure 18. The lower temperature and

reduced temperature gradients apparently provided a sample whose composition more nearly approached the equilibrium solidus composition.

Undoubtedly the most serious problem involved in using the internal molten zone technique is how to assign a reasonable oxygen pressure within the molten zone, or simply stated, what temperature should be used to calculate the oxygen pressure from the different CO/CO_2 gas mixtures. While no effort was made during this research to evaluate the mechanism whereby the various gases and/or oxygen was transmitted through the skin to the center of the sample, it became apparent that using the internal molten zone temperature gave the most consistent and realistic oxygen pressure values. Certainly the temperature controlling the oxygen potential must be between the surface temperature of the skin and the higher interior temperature of the sample. If the sample surface temperatures (some 400-500°C below the interior temperature) were utilized the consistency shown in the phase diagram, including the agreement with the extrapolation from solid CeO_{2-x} data, breaks down severely. Other investigators have used the internal molten zone technique to obtain redox equilibrium in molten $UO_{2\pm x}$[5]. They were able to use liquidus and solidus temperatures obtained from an independent investigation to calculate oxygen pressures in CO/CO_2 and H_2/H_2O gas mixtures and obtain good agreement between the molten redox

equilibrium and the extrapolated lower temperature solid $UO_{2\pm x}$ data.

Although the preceeding discussion cannot satisfy all objections to using the internal molten zone technique to determine redox equilibrium in nonstoichiometric refractory oxides, it certainly is evident that consistent and reasonable phase diagrams can be assembled for CeO_{2-x} and $UO_{2\pm x}$ using data gathered with this technique. Since the technique is usable in very high melting refractory oxides it avoids many of the material containment and contamination problems associated with any other techniques. The only limitation is the need to use oxides that possess enough high temperature electrical conductivity to support eddy current heating needed for the successful generation of a stable internal molten zone.

CHAPTER VI

CONCLUSIONS

1. The phase relations for solid CeO_{2-x} was determined at 1744°, 1587°, 1725° and 1808°C and a continuous solid solution region was found from CeO_2 to $CeO_{1.65}$ in equilibrium with oxygen pressures between 10^{-3} and 10^{-12} atmospheres. The data are presented in Figure 15.

2. The internal molten zone technique was used to establish equilibrium between molten CeO_{2-x} and oxygen pressure generated in controlled CO/CO_2 gas mixtures.

3. Liquidus temperatures were experimentally measured and combined with the molten CeO_{2-x} composition data from the internal molten zone experiments to establish the liquidus curve. The intersection of the extrapolated oxygen isobars for solid CeO_{2-x} with the oxygen pressure values for molten ceria were used to approximate the liquidus curve. This information is shown in Figure 19.

4. A phase diagram, Figure 20, for the CeO_2-Ce_2O_3 system was presented extending from 1200°C to the liquidus line showing oxygen pressure equilibrium as isobars.

5. The internal molten zone technique was reveiwed and demonstrated to be a viable method for establishing redox equilibrium in nonstoichiometric refractory oxides.

APPENDIX A

The experimental data, calculated oxygen pressures, ceria compositions, and error estimations are given in this section. Information for each individual experiment is grouped under the experiment number, "EXP NUMBER." The experiments are grouped by temperatures in increasing order. The first few lines give the temperature gas flow rates and errors in the flow rates. The oxygen pressure for the experiment was calculated and listed as log PO_2. The maximum possible errors in the oxygen pressure were calculated by combining the errors in gas flows and a 20° deviation in temperature. The minimum and maximum oxygen pressures are listed in the two lines immediately below the correct value. The ceria composition was calculated from the weights of the platinum crucible, crucible plus CeO_{2-x}, and crucible plus CeO_2. The value of n in CeO_n is printed following "CEO." An maximum error in the composition was calculated and printed as a "$\pm$" value. This error was found by assuming a 0.0002 gram error in each weighing and combining the errors to give the maximum error in the composition.

```
 G
EXP NUMBER :18
TEMP C:1477     FLOWS,  CO2:118     % ERROR:2
                        CO:370      % ERROR:2
 TEMP C      % CO2     LOG PO2        DG1/2D2
   1477     24.18      - 8.840       -  35378
   1457     23.46      - 9.068       -  35374
   1497     24.92      - 8.617       -  34880
WEIGHTS,  PI :6.2087  PI+CEO2-X :7.3216   PI+CE02 :7.3411
 CEO  1.8148     +-  0.0038
WEIGHTS,  PI :6.5434  PI+CEO2-X :8.8199   PI+CE02 :8.8592
 CEO  1.8175     +-  0.0019

EXP NUMBER :19
TEMP C:1477     FLOWS,  CO2:184     % ERROR:2
                        CO:410      % ERROR:2
 TEMP C      % CO2     LOG PO2        DG1/2D2
   1477     30.98      - 8.543       -  34191
   1457     30.13      - 8.771       -  34700
   1497     31.84      - 8.320       -  33679
WEIGHTS,  PI :6.2087  PI+CEO2-X :7.0405   PI+CE02 :7.0536
 CEO  1.8332     +-  0.0051
WEIGHTS,  PI :6.5434  PI+CEO2-X :7.5300   PI+CE02 :7.5965
 CEO  1.8315     +-  0.0041


EXP NUMBER :25
TEMP C:1477     FLOWS,  CO2:220     % ERROR:2
                        CO:340      % ERROR:2
 TEMP C      % CO2     LOG PO2        DG1/2D2
   1477     39.29      - 8.226       -  32919
   1457     38.34      - 8.453       -  33443
   1497     40.24      - 8.003       -  32392
WEIGHTS,  PI :6.5432  PI+CEO2-X :7.3129   PI+CE02 :7.3241
 CEO  1.8457     +-  0.0055
WEIGHTS,  PI :6.2086  PI+CEO2-X :7.0365   PI+CE02 :7.0485
 CEO  1.8463     +-  0.0051


EXP NUMBER :26
TEMP C:1477     FLOWS,  CO2:220     % ERROR:2
                        CO:340      % ERROR:2
 TEMP C      % CO2     LOG PO2        DG1/2D2
   1477     39.29      - 8.226       -  32919
   1457     38.34      - 8.453       -  33443
   1497     40.24      - 8.003       -  32392
WEIGHTS,  PI :6.2086  PI+CEO2-X :8.8088   PI+CE02 :8.8467
 CEO  1.8455     +-  0.0016

WEIGHTS,  PI :6.5432  PI+CEO2-X :8.8781   PI+CE02 :8.9130
 CEO  1.8416     +-  0.0018
#
```

```
EXP NUMBER :28
TEMP C:1477     FLOWS,  CO2:680     % ERROR:2
                         CO:58     % ERROR:2
 TEMP C      % CO2     LOG PO2        DG1/202
   1477     92.14      - 5.710        -  22851
   1457     91.85      - 5.937        -  23490
   1497     92.43      - 5.487        -  22209
WEIGHTS,  PT :6.2085  PT+CEO2-X :8.1391    PT+CE02 :8.1491
 CEO  1.9446     +-  0.0022
WEIGHTS,  PT :6.5431  PT+CEO2-X :10.0252    PT+CE02 :10.0447
 CEO  1.9401     +-  0.0012

EXP NUMBER :29
TEMP C:1477     FLOWS,  CO2:240     % ERROR:2
                         CO:58     % ERROR:2
 TEMP C      % CO2     LOG PO2        DG1/202
   1477     80.54      - 6.614        -  26470
   1457     79.90      - 6.842        -  27068
   1497     81.16      - 6.391        -  25870
WEIGHTS,  PT :6.5432  PT+CEO2-X :7.8416    PT+CE02 :7.8539
 CEO  1.8991     +-  0.0033
WEIGHTS,  PT :6.2085  PT+CEO2-X :11.4536    PT+CE02 :11.5023
 CEO  1.9010     +-  0.0008

EXP NUMBER :30
TEMP C:1477     FLOWS,  CO2:36     % ERROR:2
                         CO:560     % ERROR:2
 TEMP C      % CO2     LOG PO2        DG1/202
   1477      6.04      -10.231        -  40944
   1457      5.82      -10.458        -  41376
   1497      6.27      -10.008        -  40509
WEIGHTS,  PT :6.2085  PT+CEO2-X :9.5515    PT+CE02 :9.6189
 CEO  1.7874     +-  0.0013
WEIGHTS,  PT :6.5432  PT+CEO2-X :9.4961    PT+CE02 :9.5571
 CEO  1.7823     +-  0.0014

EXP NUMBER :31
TEMP C:1477     FLOWS,  CO2:36     % ERROR:2
                         CO:560     % ERROR:2
 TEMP C      % CO2     LOG PO2        DG1/202
   1477      6.04      -10.231        -  40944
   1457      5.82      -10.458        -  41376
   1497      6.27      -10.008        -  40509
WEIGHTS,  PT :6.2085  PT+CEO2-X :8.6644    PT+CE02 :8.7162
 CEO  1.7778     +-  0.0017
WEIGHTS,  PT :6.5432  PT+CEO2-X :8.3871    PT+CE02 :8.4260
 CEO  1.7778     +-  0.0023
```

```
EXP NUMBER :32
TEMP C:1477     FLOWS,  CO2:65     % ERROR:1
                         CO:582     % ERROR:1
 TEMP C      % CO2     LOG PO2        DG1/202
   1477     10.05      - 9.751        -  39025
   1457      9.87      - 9.961        -  39410
   1497     10.23      - 9.546        -  38638
WEIGHTS,  PT :6.2085  PT+CEO2-X :7.8679    PT+CE02 :7.9005
 CEO  1.7927     +-  0.0026
WEIGHTS,  PT :6.5431  PT+CEO2-X :8.1609    PT+CE02 :8.1920
 CEO  1.7971     +-  0.0026

EXP NUMBER :33
TEMP C:1477     FLOWS,  CO2:61     % ERROR:2
                         CO:939     % ERROR:2
 TEMP C      % CO2     LOG PO2        DG1/202
   1477      6.10     -10.222        -  40908
   1457      5.88     -10.449        -  41340
   1497      6.33      - 9.999       -  40473
WEIGHTS,  PT :6.2085  PT+CEO2-X :8.8716    PT+CE02 :8.9323
 CEO  1.7603     +-  0.0016
WEIGHTS,  PT :6.5432  PT+CEO2-X :8.9878    PT+CE02 :9.0433
 CEO  1.7612     +-  0.0017

EXP NUMBER :34
TEMP C:1477     FLOWS,  CO2:63     % ERROR:2
                         CO:560     % ERROR:2
 TEMP C      % CO2     LOG PO2        DG1/202
   1477     10.11      - 9.745        -  39000
   1457      9.76      - 9.972        -  39454
   1497     10.43      - 9.522        -  38542
WEIGHTS,  PT :6.2084  PT+CEO2-X :8.6495    PT+CE02 :8.7013
 CEO  1.7765     +-  0.0017
WEIGHTS,  PT :6.5431  PT+CEO2-X :9.7506    PT+CE02 :9.8185
 CEO  1.7770     +-  0.0013

EXP NUMBER :35
TEMP C:1477     FLOWS,  CO2:6.8    % ERROR:1
                         CO:93.2    % ERROR:1
 TEMP C      % CO2     LOG PO2        DG1/202
   1477      6.80     -10.121        -  40505
   1457      6.68     -10.331        -  40873
   1497      6.93      - 9.915       -  40135
WEIGHTS,  PT :6.2084  PT+CEO2-X :7.9552    PT+CE02 :7.9937
 CEO  1.7680     +-  0.0024
WEIGHTS,  PT :6.5430  PT+CEO2-X :7.6776    PT+CE02 :7.7037
 CEO  1.7581     +-  0.0037
```

```
EXP NUMBER :36
TEMP C:1477     FLOWS,  CO2:43     % ERROR:2
                        CO:860     % ERROR:2
 TEMP C      % CO2     LOG PO2       DG1/202
   1477      4.76      -10.449       -  41818
   1457      4.53      -10.677       -  42240
   1497      4.95      -10.226       -  41393
WEIGHTS,  PT :6.2082  PT+CEO2-X :8.9109   PT+CE02 :8.9720
 CEO  1.7622     +-  0.0016
WEIGHTS,  PT :6.5430  PT+CEO2-X :10.0325   PT+CE02 :10.1126
 CEO  1.7586     +-  0.0012


EXP NUMBER :37
TEMP C:1477     FLOWS,  CO2:1.1     % ERROR:2
                        CO:98.9     % ERROR:2
 TEMP C      % CO2     LOG PO2       DG1/202
   1477      1.10      -11.755       -  47042
   1457      1.06      -11.982       -  47404
   1497      1.15      -11.531       -  46677
WEIGHTS,  PT :6.2082  PT+CEO2-X :10.3972   PT+CE02 :10.5075
 CEO  1.7240     +-  0.0010
WEIGHTS,  PT :6.5430  PT+CEO2-X :10.7616   PT+CE02 :10.8734
 CEO  1.7223     +-  0.0010


EXP NUMBER :39
TEMP C:1477     FLOWS,  CO2:2.4     % ERROR:1
                        CO:97.6     % ERROR:1
 TEMP C      % CO2     LOG PO2       DG1/202
   1477      2.40      -11.066       -  44284
   1457      2.35      -11.276       -  44689
   1497      2.45      -10.860       -  43953
WEIGHTS,  PT :6.2083  PT+CEO2-X :8.9705   PT+CE02 :9.0394
 CEO  1.7382     +-  0.0015
WEIGHTS,  PT :6.5430  PT+CEO2-X :8.5533   PT+CE02 :8.6037
 CEO  1.7369     +-  0.0021


EXP NUMBER :40
TEMP C:1477     FLOWS,  CO2:0.2     % ERROR:2
                        CO:99.8     % ERROR:2
 TEMP C      % CO2     LOG PO2       DG1/202
   1477      0.20      -13.243       -  52998
   1457      0.19      -13.470       -  53292
   1497      0.21      -13.020       -  52701
WEIGHTS,  PT :6.4-6.5430  PT+CEO2-X :7.4857   PT+CE02 :7.5142
 CEO  1.6843     +-  0.0044
```

```
 G
EXP NUMBER :42
TEMP C:1477     FLOWS,  CO2:220     % ERROR:2
                        CO:355      % ERROR:2
 TEMP C      % CO2     LOG PO2        DG1/202
   1477     38.26      - 8.263       -  33069
   1457     37.32      - 8.491       -  33591
   1497     39.21      - 8.040       -  32544
WEIGHTS,  PT :6.2084  PT+CEO2-X :6.9974   PT+CE02 :7.0087
 CEO  1.8481     +-  0.0054
WEIGHTS,  PT :6.5430  PT+CEO2-X :7.6475   PT+CE02 :7.6620
 CEO  1.8606     +-  0.0039


EXP NUMBER :43
TEMP C:1477     FLOWS,  CO2:48.4    % ERROR:2
                        CO:51.6     % ERROR:2
 TEMP C      % CO2     LOG PO2        DG1/202
   1477     48.40      - 7.903       -  31629
   1457     47.40      - 8.131       -  32167
   1497     49.40      - 7.680       -  31087
WEIGHTS,  PT :6.2086  PT+CEO2-X :8.0716   PT+CE02 :8.0951
 CEO  1.8660     +-  0.0023
WEIGHTS,  PT :6.5432  PT+CEO2-X :7.8727   PT+CE02 :7.8900
 CEO  1.8618     +-  0.0032

EXP NUMBER :44
TEMP C:1477     FLOWS,  CO2:800     % ERROR:2
                        CO:35       % ERROR:2
 TEMP C      % CO2     LOG PO2        DG1/202
   1477     95.81      - 5.130       -  20532
   1457     95.64      - 5.358       -  21196
   1497     95.96      - 4.908       -  19864
WEIGHTS,  PT :6.2087  PT+CEO2-X :8.1511   PT+CE02 :8.1593
 CEO  1.9548     +-  0.0022
WEIGHTS,  PT :6.5432  PT+CEO2-X :7.8062   PT+CE02 :7.8116
 CEO  1.9542     +-  0.0034


EXP NUMBER :45
TEMP C:1477     FLOWS,  CO2:1       % ERROR:0
                        CO:99       % ERROR:1
 TEMP C      % CO2     LOG PO2        DG1/202
   1477      1.00     -11.838       -  47377
   1457      0.99     -12.040       -  47632
   1497      1.01     -11.641       -  47120
WEIGHTS,  PT :6.2087  PT+CEO2-X :8.3581   PT+CE02 :8.4159
 CEO  1.7183     +-  0.0020
WEIGHTS,  PT :6.5434  PT+CEO2-X :9.0197   PT+CE02 :9.0852
 CEO  1.7228     +-  0.0017
```

```
EXP NUMBER :79
TEMP C:1477     FLOWS,  CO2:363     % ERROR:1
                         CO:67     % ERROR:1
 TEMP C      % CO2     LOG PO2        DG1/202
   1477     84.42      - 6.380       -  25534
   1457     84.15      - 6.590       -  26073
   1497     84.68      - 6.175       -  24993
WEIGHTS,  PT :6.2089  PT+CEO2-X :8.0839   PT+CE02 :8.0962
 CEO  1.9299     +-  0.0023
WEIGHTS,  PT :6.5437  PT+CEO2-X :9.9655   PT+CE02 :9.9913
 CEO  1.9195     +-  0.0013


EXP NUMBER :80
TEMP C:1477     FLOWS,  CO2:95.8     % ERROR:2
                         CO:4.2     % ERROR:2
 TEMP C      % CO2     LOG PO2        DG1/202
   1477     95.80      - 5.132       -  20539
   1457     95.64      - 5.360       -  21204
   1497     95.96      - 4.909       -  19872
WEIGHTS,  PT :6.2089  PT+CEO2-X :7.8024   PT+CE02 :7.8086
 CEO  1.9583     +-  0.0027
WEIGHTS,  PT :6.5436  PT+CEO2-X :8.5186   PT+CE02 :8.5223
 CEO  1.9772     +-  0.0022
```

```
EXP NUMBER :57
TEMP C:1477     FLOWS,  CO2:1      % ERROR:1
                         CO:99      % ERROR:1
 TEMP C       % CO2      LOG PO2        DG1/202
   1477       1.00       -11.838        -  47377
   1457       0.93       -12.048        -  47666
   1497       1.02       -11.632        -  47085
WEIGHTS,  PT :6.2087  PT+CEO2-X :7.5381    PT+CE02 :7.5736
 CEO  1.7202     +-  0.0032
WEIGHTS,  PT :6.5435  PT+CEO2-X :8.6380    PT+CE02 :8.6930
 CEO  1.7247     +-  0.0020

EXP NUMBER :58
TEMP C:1477     FLOWS,  CO2:96.4     % ERROR:2
                         CO:3.6     % ERROR:2
 TEMP C       % CO2      LOG PO2        DG1/202
   1477      96.40       - 4.993        -  19982
   1457      96.26       - 5.220        -  20653
   1497      96.53       - 4.770        -  19309
WEIGHTS,  PT :6.2088  PT+CEO2-X :9.2280    PT+CE02 :9.2410
 CEO  1.9539     +-  0.0014
WEIGHTS,  PT :6.5433  PT+CEO2-X :9.1965    PT+CE02 :9.2086
 CEO  1.9512     +-  0.0016

EXP NUMBER :64
TEMP C:1477     FLOWS,  CO2:822     % ERROR:3
                         CO:29.7     % ERROR:1
 TEMP C       % CO2      LOG PO2        DG1/202
   1477      96.51       - 4.964        -  19868
   1457      96.37       - 5.192        -  20541
   1497      96.64       - 4.742        -  19195
WEIGHTS,  PT :6.2087  PT+CEO2-X :7.8961    PT+CE02 :7.9007
 CEO  1.9708     +-  0.0026
WEIGHTS,  PT :6.5432  PT+CEO2-X :7.7005    PT+CE02 :7.7051
 CEO  1.9574     +-  0.0037

EXP NUMBER :78
TEMP C:1477     FLOWS,  CO2:59      % ERROR:2
                         CO:41      % ERROR:2
 TEMP C       % CO2      LOG PO2        DG1/202
   1477      59.00       - 7.532        -  30141
   1457      58.03       - 7.759        -  30697
   1497      59.97       - 7.308        -  29583
WEIGHTS,  PT :6.2088  PT+CEO2-X :9.3946    P1+CE02 :9.4330
 CEO  1.8719     +-  0.0013
WEIGHTS,  PT :6.5435  PT+CEO2-X :9.7049    PT+CE02 :9.7428
 CEO  1.8726     +-  0.0014
```

```
EXP NUMBER :79
TEMP. C:1477     FLOWS,  CO2:363     % ERROR:1
                          CO:67     % ERROR:1
 TEMP C      % CO2     LOG PO2        DG1/202
   1477     84.42      - 6.380        -  25534
   1457     84.15      - 6.590        -  26073
   1497     84.68      - 6.175        -  24993
WEIGHTS,  PT :6.2089  PT+CEO2-X :8.0839   PT+CE02 :8.0962
 CEO  1.9299     +-  0.0023
WEIGHTS,  PT :6.5437  PT+CEO2-X :9.9655   PT+CE02 :9.9913
 CEO  1.9195     +-  0.0013


EXP NUMBER :80
TEMP C:1477     FLOWS,  CO2:95.8     % ERROR:2
                          CO:4.2     % ERROR:2
 TEMP C      % CO2     LOG PO2        DG1/202
   1477     95.80      - 5.132        -  20539
   1457     95.64      - 5.360        -  21204
   1497     95.96      - 4.909        -  19872
WEIGHTS,  PT :6.2089  PT+CEO2-X :7.8024   PT+CE02 :7.8086
 CEO  1.9583     +-  0.0027
WEIGHTS,  PT :6.5436  PT+CEO2-X :8.5186   PT+CE02 :8.5223
 CEO  1.9772     +-  0.0022
```

```
G
EXP NUMBER :60
TEMP C:1587     FLOWS,  CO2:1      % ERROR:1
                        CO:99      % ERROR:1
 TEMP C      % CO2     LOG PO2        DG1/202
   1587      1.00      -10.853        -  46166
   1567      0.98      -11.041        -  46459
   1607      1.02      -10.670        -  45872
WEIGHTS,  PI :6.2088  PI+CEO2-X :9.1959    PI+CE02 :9.2834
 CEO  1.6939     +-  0.0014
WEIGHTS,  PI :6.5434  PI+CEO2-X :8.3220    PI+CE02 :8.3731
 CEO  1.6996     +-  0.0024


EXP NUMBER :61
TEMP C:1587     FLOWS,  CO2:561     % ERROR:2
                        CO:39      % ERROR:2
 TEMP C      % CO2     LOG PO2        DG1/202
   1587     86.31      - 5.264        -  22391
   1567     85.83      - 5.469        -  23012
   1607     86.77      - 5.063        -  21767
WEIGHTS,  PI :6.5432  PI+CEO2-X :7.7431    PI+CE02 :7.7533
 CEO  1.9093     +-  0.0036
WEIGHTS,  PI :6.2087  PI+CEO2-X :7.9048    PI+CE02 :7.9195
 CEO  1.9076     +-  0.0025


 EXP NUMBER :62
 TEMP C:1587     FLOWS,  CO2:239     % ERROR:2
                         CO:256     % ERROR:2
  TEMP C      % CO2     LOG PO2        DG1/202
    1587     48.28      - 6.923        -  29446
    1567     47.29      - 7.127        -  29991
    1607     49.28      - 6.721        -  28897
 WEIGHTS,  PI :6.2086  PI+CEO2-X :7.2561    PI+CE02 :7.2705
  CEO  1.8541     +-  0.0041
 WEIGHTS,  PI :6.5432  PI+CEO2-X :7.9721    PI+CE02 :7.9913
  CEO  1.8574     +-  0.0030


 EXP NUMBER :63
 TEMP C:1587     FLOWS,  CO2:40     % ERROR:2
                         CO:467     % ERROR:2
  TEMP C      % CO2     LOG PO2        DG1/202
    1587      7.89      - 8.997        -  38270
    1567      7.60      - 9.202        -  38720
    1607      8.19      - 8.796        -  37816
 WEIGHTS,  PI :6.2088  PI+CEO2-X :8.0732    PI+CE02 :8.1131
  CEO  1.7746     +-  0.0023
 WEIGHTS,  PI :6.5434  PI+CEO2-X :8.6474    PI+CE02 :8.6911
  CEO  1.7811     +-  0.0020
```

```
EXP NUMBER :72
TEMP C:1587     FLOWS,  CO2:1      % ERROR:1
                        CO:99      % ERROR:1
 TEMP C       % CO2      LOG PO2        DG1/202
   1587       1.00       -10.853        -  46166
   1567       0.98       -11.041        -  46459
   1607       1.02       -10.670        -  45872
WEIGHTS,  PT :6.2086  PT+CEO2-X :8.5243   PT+CE02 :8.5895
 CEO  1.7054     +-  0.0018
WEIGHTS,  PT :6.5430  PT+CEO2-X :8.4884   PT+CE02 :8.5444
 CEO  1.6990     +-  0.0022


EXP NUMBER :73
TEMP C:1587     FLOWS,  CO2:31     % ERROR:2
                        CO:664     % ERROR:4
 TEMP C       % CO2      LOG PO2        DG1/202
   1587       4.46       - 9.524        -  40511
   1567       4.21       - 9.746        -  41009
   1607       4.73       - 9.305        -  40005
WEIGHTS,  PT :6.2087  PT+CEO2-X :7.2573   PT+CE02 :7.2817
 CEO  1.7554     +-  0.0040
WEIGHTS,  PT :6.5430  PT+CEO2-X :7.9053   PT+CE02 :7.9363
 CEO  1.7607     +-  0.0031


EXP NUMBER :74
TEMP C:1587     FLOWS,  CO2:615    % ERROR:4
                        CO:26      % ERROR:4
 TEMP C       % CO2      LOG PO2        DG1/202
   1587      95.92       - 4.119        -  17520
   1567      95.61       - 4.357        -  18334
   1607      96.21       - 3.886        -  16706
WEIGHTS,  PT :6.2086  PT+CEO2-X :8.5031   PT+CE02 :8.5144
 CEO  1.9473     +-  0.0019
WEIGHTS,  PT :6.5430  PT+CEO2-X :8.7345   PT+CE02 :8.7432
 CEO  1.9575     +-  0.0020


EXP NUMBER :81
TEMP C:1587     FLOWS,  CO2:206    % ERROR:4
                        CO:295     % ERROR:4
 TEMP C       % CO2      LOG PO2        DG1/202
   1587      41.12       - 7.175        -  30518
   1567      39.20       - 7.414        -  31199
   1607      43.07       - 6.939        -  29832
WEIGHTS,  PT :6.2090  PT+CEO2-X :8.5929   PT+CE02 :8.6300
 CEO  1.8351     +-  0.0018
WEIGHTS,  PT :6.5434  PT+CEO2-X :9.5222   PT+CE02 :9.5679
 CEO  1.8375     +-  0.0014
```

```
EXP NUMBER :82
TEMP C:1587     FLOWS,  CO2:28.8     % ERROR:2
                        CO:71.2      % ERROR:2
 TEMP C      % CO2     LOG PO2        DG1/202
   1587     28.80      - 7.649       -  32535
   1567     27.99      - 7.854       -  33047
   1607     29.63      - 7.448       -  32020
WEIGHTS,  PT :6.2085  PT+CEO2-X :7.7144   PT+CE02 :7.4+7.7411
 CEO  1.8126     +-  0.0028
WEIGHTS,  PT :6.5434  PT+CEO2-X :8.1916   PT+CE02 :8.2220
 CEO  1.8052     +-  0.0026


EXP NUMBER :83
TEMP C:1587     FLOWS,  CO2:214     % ERROR:4
                        CO:555      % ERROR:4
 TEMP C      % CO2     LOG PO2        DG1/202
   1587     27.83      - 7.691       -  32712
   1567     26.25      - 7.930       -  33369
   1607     29.47      - 7.455       -  32049
WEIGHTS,  PT :6.2086  PT+CEO2-X :8.3398   PT+CE02 :8.3767
 CEO  1.8169     +-  0.0020
WEIGHTS,  PT :6.5432  PT+CEO2-X :9.4021   PT+CE02 :9.4518
 CEO  1.8162     +-  0.0015


EXP NUMBER :84
TEMP C:1587     FLOWS,  CO2:17     % ERROR:4
                        CO:83      % ERROR:4
 TEMP C      % CO2     LOG PO2        DG1/202
   1587     17.00      - 8.240       -  35049
   1567     15.90      - 8.480       -  35681
   1607     18.16      - 8.004       -  34411
WEIGHTS,  PT :6.2085  PT+CEO2-X :7.4177   PT+CE02 :7.4404
 CEO  1.8018     +-  0.0035
WEIGHTS,  PT :6.5433  PT+CEO2-X :7.5992   PT+CE02 :7.6185
 CEO  1.8069     +-  0.0040


EXP NUMBER :85
TEMP C:1587     FLOWS,  CO2:339     % ERROR:2
                        CO:133      % ERROR:2
 TEMP C      % CO2     LOG PO2        DG1/202
   1587     71.82      - 6.050       -  25736
   1567     71.01      - 6.255       -  26321
   1607     72.63      - 5.849       -  25147
WEIGHTS,  PT :6.2088  PT+CEO2-X :7.6031   PT+CE02 :7.6198
 CEO  1.8727     +-  0.0031
WEIGHTS,  PT :6.5462  PT+CEO2-X :8.0407   PT+CE02 :8.0580
 CEO  1.8769     +-  0.0029
```

```
EXP NUMBER :86
TEMP C:1537     FLOWS,  CO2:2.2     % ERROR:1
                         CO:97.8     % ERROR:1
 TEMP C      % CO2     LOG PO2        DG1/2D2
   1587      2.20      -10.158        -  43208
   1567      2.16      -10.346        -  43533
   1607      2.24      - 9.974        -  42882
WEIGHTS,  PT :6.2037  PT+CEO2-X :7.2368   PT+CE02 :7.2635
 CEO  1.7277     +-  0.0041
WEIGHTS,  PT :6.5434  PT+CEO2-X :7.8982   PT+CE02 :7.9347
 CEO  1.7178     +-  0.0031


EXP NUMBER :87
TEMP C:1537     FLOWS,  CO2:.0-0.2     % ERROR:2
                         CO:99.8     % ERROR:2
 TEMP C      % CO2     LOG PO2        DG1/2D2
   1587      0.20      -12.258        -  52141
   1567      0.19      -12.463        -  52442
   1607      0.21      -12.057        -  51836
WEIGHTS,  PT :6.2035  PT+CEO2-X :7.5278   PT+CE02 :7.5692
 CEO  1.6727     +-  0.0032
WEIGHTS,  PT :6.5429  PT+CEO2-X :9.2764   PT+CE02 :9.3619
 CEO  1.6737     +-  0.0015

EXP NUMBER :88
TEMP C:1537     FLOWS,  CO2:94.2     % ERROR:2
                         CO:5.8     % ERROR:2
 TEMP C      % CO2     LOG PO2        DG1/2D2
   1587     94.19      - 4.443        -  18900
   1567     93.97      - 4.648        -  19556
   1607     94.40      - 4.243        -  18241
WEIGHTS,  PT :6.2084  PT+CEO2-X :7.9164   PT+CE02 :7.9262
 CEO  1.9386     +-  0.0025
WEIGHTS,  PT :6.5432  PT+CEO2-X :9.3098   PT+CE02 :9.3256
 CEO  1.9389     +-  0.0016
```

```
EXP NUMBER :89
TEMP C:1725     FLOWS,  CO2:532     % ERROR:2
                        CO:56.5     % ERROR:2
 TEMP C      % CO2     LOG PO2       DG1/202
   1725     90.36      - 3.839       -  17541
   1705     90.02      - 4.020       -  18183
   1745     90.68      - 3.662       -  16900
WEIGHTS,  PT :6.2087  PT+CEO2-X :8.8205   PT+CE02 :8.8453
 CEO  1.8988     +-  0.0016
WEIGHTS,  PT :6.5435  PT+CEO2-X :8.1513   PT+CE02 :8.1668
 CEO  1.8973     +-  0.0027


EXP NUMBER :90
TEMP C:1725     FLOWS,  CO2:241     % ERROR:2
                        CO:57       % ERROR:2
 TEMP C      % CO2     LOG PO2       DG1/202
   1725     80.87      - 4.532       -  20706
   1705     80.24      - 4.713       -  21321
   1745     81.47      - 4.353       -  20090
WEIGHTS,  PT :6.2083  PT+CEO2-X :8.8884   PT+CE02 :8.9210
 CEO  1.8707     +-  0.0016
WEIGHTS,  PT :6.5435  PT+CEO2-X :9.1562   PT+CE02 :9.2169
 CEO  1.8765     +-  0.0016


EXP NUMBER :92
TEMP C:1725     FLOWS,  CO2:225     % ERROR:2
                        CO:556      % ERROR:2
 TEMP C      % CO2     LOG PO2       DG1/202
   1725     28.81      - 6.569       -  30016
   1705     28.00      - 6.751       -  30537
   1745     29.64      - 6.391       -  29492
WEIGHTS,  PT :6.2086  PT+CEO2-X :8.2466   PT+CE02 :8.2874
 CEO  1.7889     +-  0.0021
WEIGHTS,  PT :6.5431  PT+CEO2-X :8.8351   PT+CE02 :8.8794
 CEO  1.7960     +-  0.0019


EXP NUMBER :93
TEMP C:1725     FLOWS,  CO2:199.6   % ERROR:2
                        CO:563      % ERROR:2
 TEMP C      % CO2     LOG PO2       DG1/202
   1725     26.17      - 6.684       -  30541
   1705     25.41      - 6.866       -  31057
   1745     26.95      - 6.505       -  30022
WEIGHTS,  PT :6.2035  PT+CEO2-X :7.7911   PT+CE02 :7.8227
 CEO  1.7894     +-  0.0027
WEIGHTS,  PT :6.5433  PT+CEO2-X :7.6300   PT+CE02 :7.6510
 CEO  1.7961     +-  0.0039
```

```
EXP NUMBER :94
TEMP C:1725     FLOWS,  CO2:230     % ERROR:2
                         CO:355     % ERROR:2
 TEMP C      % CO2     LOG PO2        DG1/202
   1725     39.32      - 6.161       -  28148
   1705     38.37      - 6.342       -  28688
   1745     40.28      - 5.982       -  27605
WEIGHTS,  PT :6.2087  PT+CEO2-X :7.9323   PT+CE02 :7.9621
 CEO  1.8172     +-  0.0025
WEIGHTS,  PT :6.5433  PT+CEO2-X :8.3290   PT+CE02 :8.3597
 CEO  1.8182     +-  0.0024


EXP NUMBER :95
TEMP C:1725     FLOWS,  CO2:336     % ERROR:2
                         CO:230     % ERROR:2
 TEMP C      % CO2     LOG PO2        DG1/202
   1725     59.36      - 5.454       -  24922
   1705     58.40      - 5.636       -  25495
   1745     60.32      - 5.276       -  24347
WEIGHTS,  PT :6.2084  PT+CEO2-X :8.8079   PT+CE02 :8.8444
 CEO  1.8511     +-  0.0016
WEIGHTS,  PT :6.5434  PT+CEO2-X :9.3643   PT+CE02 :9.4061
 CEO  1.8429     +-  0.0015


EXP NUMBER :96
TEMP C:1725     FLOWS,  CO2:0.3     % ERROR:2
                         CO:99.7     % ERROR:4
 TEMP C      % CO2     LOG PO2        DG1/202
   1725      0.30      -10.826       -  49465
   1705      0.28      -11.024       -  49863
   1745      0.32      -10.629       -  49053
WEIGHTS,  PT :6.2085  PT+CEO2-X :8.4535   PT+CE02 :8.5287
 CEO  1.6513     +-  0.0019
WEIGHTS,  PT :6.5432  PT+CEO2-X :8.3384   PT+CE02 :8.3981
 CEO  1.6538     +-  0.0023


EXP NUMBER :104
TEMP C:1725     FLOWS,  CO2:13.5    % ERROR:2
                         CO:410     % ERROR:4
 TEMP C      % CO2     LOG PO2        DG1/202
   1725      3.19      - 8.748       -  39971
   1705      3.01      - 8.947       -  40469
   1745      3.38      - 8.551       -  39463
WEIGHTS,  PT :6.2079  PT+CEO2-X :8.2825   PT+CE02 :8.3401
 CEO  1.7094     +-  0.0020
WEIGHTS,  PT :6.5429  PT+CEO2-X :8.8755   PT+CE02 :8.9400
 CEO  1.7105     +-  0.0018
```

```
EXP NUMBER :105
TEMP C:1725     FLOWS,  CO2:48      % ERROR:2
                         CO:410      % ERROR:4
 TEMP C       % CO2      LOG PO2        DG1/2D2
   1725      10.48       - 7.646        -  34937
   1705       9.94       - 7.845        -  35486
   1745      11.06       - 7.450        -  34380
WEIGHTS,  PT :6.2082  PT+CEO2-X :7.6434   PT+CE02 :7.6764
 CEO  1.7582      +-  0.0029
WEIGHTS,  PT :6.5429  PT+CEO2-X :8.5335   PT+CE02 :8.5792
 CEO  1.7586      +-  0.0021


EXP NUMBER :106
TEMP C:1725     FLOWS,  CO2:4.5     % ERROR:2
                         CO:95.5     % ERROR:2
 TEMP C       % CO2      LOG PO2        DG1/2D2
   1725       4.50       - 8.437        -  38548
   1705       4.33       - 8.618        -  38985
   1745       4.68       - 8.258        -  38110
WEIGHTS,  PT :6.2080  PT+CEO2-X :8.4095   PT+CE02 :8.4667
 CEO  1.7276      +-  0.0019
WEIGHTS,  PT :6.5428  PT+CEO2-X :8.5299   PT+CE02 :8.5811
 CEO  1.7298      +-  0.0021


EXP NUMBER :107
TEMP C:1725     FLOWS,  CO2:1       % ERROR:1
                         CO:99       % ERROR:1
 TEMP C       % CO2      LOG PO2        DG1/2D2
   1725       1.00       - 9.774        -  44659
   1705       0.98       - 9.938        -  44956
   1745       1.02       - 9.613        -  44362
WEIGHTS,  PT :6.2084  PT+CEO2-X :8.5698   PT+CE02 :8.6431
 CEO  1.6761      +-  0.0018
WEIGHTS,  PT :6.5431  PT+CEO2-X :8.3183   PT+CE02 :8.3719
 CEO  1.6847      +-  0.0024
```

```
EXP NUMBER :97
TEMP C:1808     FLOWS,  CO2:239     % ERROR:4
                         CO:59.3     % ERROR:4
 TEMP C      % CO2     LOG PO2        DG1/202
   1808     80.09      - 3.995        - 19012
   1788     78.80      - 4.199        - 19793
   1828     81.32      - 3.794        - 18227
WEIGHTS,  PT :6.2083  PT+CEO2-X :7.8628   PT+CE02 :7.8850
 CEO  1.8576     +-  0.0026
WEIGHTS,  PT :6.5431  PT+CEO2-X :8.0162   PT+CE02 :8.0362
  CEO  1.8559     +-  0.0029


EXP NUMBER :98
TEMP C:1808     FLOWS,  CO2:450     % ERROR:4
                         CO:62      % ERROR:4
 TEMP C      % CO2     LOG PO2        DG1/202
   1808     87.80      - 3.488        - 16601
   1788     86.95      - 3.691        - 17396
   1828     88.57      - 3.290        - 15807
WEIGHTS,  PT :6.2084  PT+CEO2-X :8.1922   PT+CE02 :8.2166
 CEO  1.8682     +-  0.0022
WEIGHTS,  PT :6.5431  PT+CEO2-X :9.2501   PT+CE02 :9.2323
 CEO  1.8735     +-  0.0016


EXP NUMBER :99
TEMP C:1808     FLOWS,  CO2:220     % ERROR:5
                         CO:245     % ERROR:2
 TEMP C      % CO2     LOG PO2        DG1/202
   1808     47.31      - 5.298        - 25212
   1788     45.54      - 5.495        - 25899
   1828     49.03      - 5.105        - 24529
WEIGHTS,  PT :6.2083  PT+CEO2-X :9.2606   PT+CE02 :9.3149
 CEO  1.8120     +-  0.0014
WEIGHTS,  PT :6.5432  PT+CEO2-X :9.7795   PT+CE02 :9.8374
 CEO  1.8109     +-  0.0013


EXP NUMBER :100
TEMP C:1808     FLOWS,  CO2:62      % ERROR:4
                         CO:465     % ERROR:4
 TEMP C      % CO2     LOG PO2        DG1/202
   1808     11.77      - 6.954        - 33095
   1788     10.96      - 7.159        - 33742
   1828     12.62      - 6.752        - 32441
WEIGHTS,  PT :6.2084  PT+CEO2-X :8.8536   PT+CE02 :8.9153
 CEO  1.7548     +-  0.0016
WEIGHTS,  PT :6.5431  PT+CEO2-X :9.3599   PT+CE02 :9.4255
 CEO  1.7552     +-  0.0015
```

```
EXP NUMBER :103
TEMP C:1808     FLOWS,  CO2:13.5     % ERROR:4
                         CO:410     % ERROR:4
 TEMP C       % CO2      LOG PO2        DG1/202
   1808       3.19       - 8.169        -  38875
   1788       2.95       - 8.374        -  39466
   1828       3.45       - 7.967        -  38277
WEIGHTS,  PT :6.2083  PT+CEO2-X :9.9+9.0917    PT+CE02 :9.1718
 CEO  1.7092     +-  0.0015
WEIGHTS,  PT :6.5428  PT+CEO2-X :8.3771    PT+CE02 :8.4279
 CEO  1.7101     +-  0.0023


EXP NUMBER :108
TEMP C:1808     FLOWS,  CO2:1     % ERROR:1
                         CO:99     % ERROR:1
 TEMP C       % CO2      LOG PO2        DG1/202
   1808       1.00       - 9.195        -  43758
   1788       0.98       - 9.345        -  44057
   1828       1.02       - 9.045        -  43458
WEIGHTS,  PT :6.2084  PT+CEO2-X :8.9151    PT+CE02 :9.0030
 CEO  1.6616     +-  0.0015
WEIGHTS,  PT :6.5428  PT+CEO2-X :7.6932    PT+CE02 :7.7316
 CEO  1.6525     +-  0.0036


EXP NUMBER :109
TEMP C:1808     FLOWS,  CO2:231     % ERROR:4
                         CO:559     % ERROR:2
 TEMP C       % CO2      LOG PO2        DG1/202
   1808      29.24       - 5.972        -  28420
   1788      28.00       - 6.160        -  29032
   1828      30.49       - 5.788        -  27807
WEIGHTS,  PT :6.2084  PT+CEO2-X :9.1958    PT+CE02 :9.2575
 CEO  1.7823     +-  0.0014
WEIGHTS,  PT :6.5427  PT+CEO2-X :8.6238    PT+CE02 :8.6659
 CEO  1.7867     +-  0.0020
```

```
 G
EXP NUMBER :46
TEMP C:1850     FLOWS,  CO2:1.0     % ERROR:1
                         CO:99      % ERROR:1
 TEMP C      % CO2     LOG PO2        DG1/202
   1850      1.00      - 8.920        -  43304
   1840      0.98      - 9.001        -  43496
   1860      1.02      - 8.838        -  43112
WEIGHTS,  PT :6.5434  PT+CEO2-X :7.9891   PT+CE02 :8.0454
 CEO  1.5968     +-  0.0029
WEIGHTS,  PT :6.2087  PT+CEO2-X :7.7840   PT+CE02 :7.8354
 CEO  1.6601     +-  0.0027

EXP NUMBER :47
TEMP C:1850     FLOWS,  CO2:1.0     % ERROR:1
                         CO:99      % ERROR:1
 TEMP C      % CO2     LOG PO2        DG1/202
   1850      1.00      - 8.920        -  43304
   1840      0.98      - 9.001        -  43496
   1860      1.02      - 8.838        -  43112
WEIGHTS,  PT :6.2098  PT+CEO2-X :8.0976   PT+CE02 :8.1705
 CEO  1.6000     +-  0.0022
WEIGHTS,  PT :6.5434  PT+CEO2-X :8.4617   PT+CE02 :8.5386
 CEO  1.5854     +-  0.0022
#G


EXP NUMBER :110
TEMP C:1930     FLOWS,  CO2:32.3    % ERROR:2
                         CO:576     % ERROR:2
 TEMP C      % CO2     LOG PO2        DG1/202
   1930      5.31      - 6.936        -  34943
   1920      5.11      - 7.031        -  35259
   1940      5.52      - 6.842        -  34626
WEIGHTS,  PT :6.2080  PT+CEO2-X :10.7084  PT+CE02 :10.8635
 CEO  1.6416     +-  0.0009
WEIGHTS,  PT :6.5426  PT+CEO2-X :8.8798   PT+CE02 :8.9386
 CEO  1.7360     +-  0.0018
#G


 EXP NUMBER :111
 TEMP C:1970     FLOWS,  CO2:63     % ERROR:2
                          CO:566    % ERROR:2
  TEMP C      % CO2     LOG PO2        DG1/202
    1970     10.02      - 6.107        -  31325
    1960      9.66      - 6.199        -  31657
    1980     10.38      - 6.015        -  30991
 WEIGHTS,  PT :6.2082  PT+CEO2-X :8.9117   PT+CE02 :8.9991
  CEO  1.6631     +-  0.0016
 WEIGHTS,  PT :6.5431  PT+CEO2-X :8.7542   PT+CE02 :8.8232
  CEO  1.6745     +-  0.0019
 #G
```

```
EXP NUMBER :112
TEMP C:2010     FLOWS,  CO2:62.3     % ERROR:2
                         CO:338      % ERROR:2
 TEMP C      % CO2      LOG PO2        DG1/202
   2010     15.56       - 5.443        -  28419
   2000     15.05       - 5.534        -  28764
   2020     16.10       - 5.353        -  28072
WEIGHTS,  PT :6.5429  PT+CEO2-X :9.1772   PT+CE02 :9.2547
 CEO  1.6926     +-  0.0016
WEIGHTS,  PT :
?00200003.02
#G


EXP NUMBER :115
TEMP C:2050     FLOWS,  CO2:29.5     % ERROR:1
                         CO:70.5     % ERROR:1
 TEMP C      % CO2      LOG PO2        DG1/202
   2050     29.49       - 4.514        -  23979
   2040     29.08       - 4.585        -  24251
   2060     29.91       - 4.443        -  23706
WEIGHTS,  PT :6.2075  PT+CEO2-X :9.3705   PT+CE02 :9.4574
 CEO  1.7124     +-  0.0013
WEIGHTS,  PT :6.5422  PT+CEO2-X :9.5425   PT+CE02 :9.6233
 CEO  1.7162     +-  0.0014
#G


EXP NUMBER :116
TEMP C:2070     FLOWS,  CO2:187.6     % ERROR:1
                         CO:323.2     % ERROR:2
 TEMP C      % CO2      LOG PO2        DG1/202
   2070     36.71       - 4.124        -  22096
   2060     36.02       - 4.203        -  22421
   2080     37.41       - 4.046        -  21769
WEIGHTS,  PT :6.5424  PT+CEO2-X :10.1885   PT+CE02 :10.2826
 CEO  1.7294     +-  0.0012
WEIGHTS,  PT :6.2076  PT+CEO2-X :11.0715   PT+CE02 :11.1531
 CEO  1.8225     +-  0.0009
#G


EXP NUMBER :117
TEMP C:2130     FLOWS,  CO2:343     % ERROR:1
                         CO:220     % ERROR:2
 TEMP C      % CO2      LOG PO2        DG1/202
   2130     60.64       - 2.966        -  16298
   2120     59.97       - 3.041        -  16639
   2140     61.30       - 2.892        -  15957
WEIGHTS,  PT :6.2037  PT+CEO2-X :7.4522   PT+CE02 :7.4800
 CEO  1.7657     +-  0.0034
WEIGHTS,  PT :6.5370  PT+CEO2-X :8.2464   PT+CE02 :8.2862
 CEO  1.7552     +-  0.0025
#
```

APPENDIX B

This appendix contains a copy of the computer program used to calculate the information in Appendix A. The language is FOCAL and the program was run on a PDP-8 computer.

```
 W
C FOCL/F  05/08/72

01.01 E
01.03 A "EXP NUMBER " E ,!
01.04 A "TEMP C"TC, "   FLOWS,  CO2"CD,"    % ERROR"AD,!
01.05 A "                        CO"CM,"    % ERROR"AM,!
01.15 S M(15)=58241; S N(15)=94728
01.16 S M(16)=60284; S N(16)=94739
01.17 S M(17)=62315; S N(17)=94746
01.18 S M(18)=64337; S N(18)=94750
01.19 S M(19)=66349; S N(19)=94751
01.20 S M(20)=68353; S N(20)=94752
01.21 S M(21)=70346; S N(21)=94746
01.22 S M(22)=72335; S N(22)=94744
01.23 S M(23)=74311; S N(23)=94735
01.24 S M(24)=76282; S N(24)=94724
01.25 S M(25)=78247; S N(25)=94714
01.26 S M(26)=80202; S N(26)=94698
01.27 S M(27)=82153; S N(27)=94683
01.45 C THERMO DATA IS FROM JANAF TABLES
01.46 T " TEMP C      % CO2    LOG PO2        DG1/2O2",!
01.49 S CT=CM+CD; S C1=CM/CT; S C2=CD/CT
01.50 F J=1,1,1; DO 2.0
01.55 S C1=CM+.01*AM*CM; S C2=CD-.01*AD*CD
01.57 S CT=C1+C2; S C1=C1/CT; S C2=C2/C1
01.60 S TC=TC-10; F J=1,1,1; DO 2.0
01.65 S C1=CM-.01*AM*CM; S C2=CD+.01*AD*CD
01.67 S CT=C1+C2; S C1=C1/CT; S C2=C2/CT
01.70 S TC=TC+20; F J=1,1,1; DO 2.0
01.80 GOTO 3.01

02.01 S TK=TC+273
02.02 I (3200-TK)2. I (TK-800)2.97;
02.05 S Y= FITR(TK*.01)
02.10 S D1=M(Y) +.01* (TK-Y*100)*(M(Y+1)-M(Y) )
02.20 S D2=N(Y) +.01* (TK-Y*100)*(N(Y+1)-N(Y) )
02.30 S DR= -2*(D1 - D2 )
02.32 S LKP= DR/( -1.987 *  TK )
02.34 S KP = FEXP(LKP)
02.40 S POA = KP *(C2/C1)↑2
02.43 S LA= FLOG(POA)/2.303
02.50 S P2= C2 - 2*POA ; S P1= C1 + 2*POA ; S PT=P2 +P1 + POA
02.55 S C1= P1/PT; S C2=P2/PT; S POA= POA/PT
02.60 S P= KP*(C2/C1)↑2
02.63 S LP =FLOG(P) /2.303
02.80 I (.01 - FABS(LA-LP))2.40,2.85,2.85
02.85 S G=0.5*1.986*TK*2.303*LP
02.89 S C2=100*C2
02.90 T %5.0 TC,%6.02 C2, "    "%5.03 LP, "     "%7,G,!
02.91 R
02.97 T " PROGRAM DOES NOT HAVE THERMO FOR THIS TEMP" ; Q

03.01 S I= 1+ I ; IF (2-I)3.50;
03.02 A "WEIGHTS,  PT "PT, " PT+CEO2-X "CX, "  PT+CE02 " CD ,!
03.03 S X =2-10.757828*(CD-CX)/(CD-PT)
03.05 S Z=X-2+10.757828*(CD-CX+.0004)/(CD-PT)
03.10 T %5.04 " CEO"X, "    +-" Z,!
03.15 GOTO 3.01
03.50 Q
03.55 C NUMBER IN LINE 3.03 IS MWT CEO2 / AWT OXYGEN
#
```

APPENDIX C

The results of Panlener[24,25] for CeO_{2-x}-oxygen pressure equilibrium from 700° to 1500°C were replotted in Figure 21. The axes of Figure 21 differ from those in Panlener's presentation of the phase relations. The tabulated data in the appendix of Panlener's report[24] was used to prepare Figure 21.

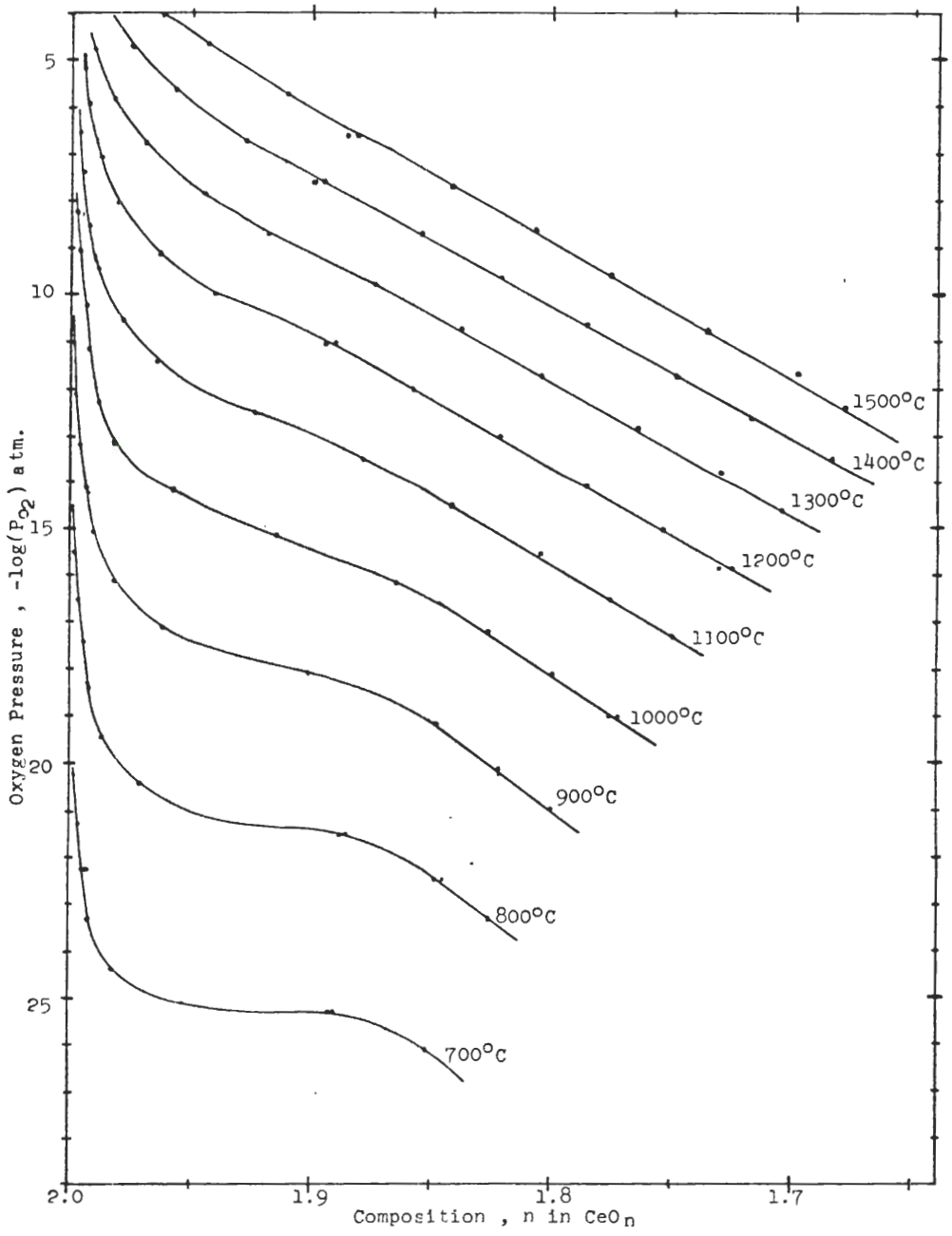

Figure 21. Isotherms for Solid CeO_{2-x} - Oxygen Pressure Equilibrium of Panlener[24].

BIBLIOGRAPHY

1. Chapman, A. T., et al., Melt-Grown Oxide-Metal Composites, Final Technical Report, ARPA Order Number 1637, December 1973.

2. Darken, L. S. and Gurry, R. W., "The System Iron-Oxygen. I. The Wustite Field and Related Equilibria," J. Am. Chem. Soc., 67, 1398-1412, 1945.

3. Darken, L. S. and Gurry, R. W., "The System Iron-Oxygen. II. Equilibrium and Thermodynamics of Liquid Oxide and Other Phases," J. Am. Chem. Soc., 68, 798-816, 1946

4. Chapman, A. T. and Meadows, R. E., "Volatility of UO_{2+x} and Phase Relations in the System Uranium-Oxygen," J. Am. Cer. Soc., 47, 614-621, 1964.

5. Chapman, A. T., Brynestad, J., and Clark, G. W., "Redox Equilibria in Molten Urania and the System U - O Above 1200°C," paper presented at the Pacific Coast Meeting of the American Ceramic Society, Nov. 2, 1976, submitted for publication to J. Am. Cer. Soc.

6. Levin, E. M., et al., Phase Diagrams for Ceramists, 1969 Supplement, Figures 2069, 2070 and 2084.

7. Rammelsberg, C., "Uber die Oxyde des Cers and die Sulfate des Ceroxydoxyduls," Ann. Phys. Chemic, Ser. 2, 108, 40-64, 1859.

8. Sterba, J., "Preparation de l'oxyde de cerium pur," C. R. Acad. Sci. (Paris), 133, 221-223, 1901.

9. Meyer, R., "Die Reindarstallung des Cerdioxyds and seinc Reduktion in Wasserstoffstrome, Z. Anorg, Chem., 37, 378-393, 1903.

10. Schenck, R. and Roter, H., "Uber die Aktivierung von Oxyden durch Fredoxyde," Z. Anorg, Chem., 211, 65-82, 1933.

11. Foex, M., "Etude dilatometrique du bioxyde et de l'oxyde bleu de cerium," C. R. Acad. Sci. (Paris), 222, 660-661, 1946.

12. Bruno, M., "Soluzioni solide anomaledi sesquiossido in biossido di cerio," Ric. Sci., 20, 645-647, 1950.

13. Richacker, G. and Birckenstaedt, M., "Natiz uber die Reduktion des Cerdioxyds insbesondere bei 250-350°C," Z. Anaorg, Chem., 265, 99-104, 1951.

14. Courtel, P. and Loriers, J., "Sur la formation de Ce_2O_3 cubique dans l'oxydation du cerium et sa mise en evidence par diffraction electronique," C. R. Acad, Sci. (Paris), 230, 735-737, 1950.

15. Brauer, Von G. and Gradinger, H., "The Oxide Systems of Cerium and Praseodymium," (in German), Z. Anorg, Chem., 277, 89-95, 1954.

16. Bevan, D. J. M., "Ordered Intermediate Phases in the System CeO_2-Ce_2O_3," J. Inorg, Nucl. Chem., 49-59, 1955.

17. Brauer, G. and Gingerich, K. A., "Uber die Oxyde des Cers-V, Hochtemperatur-Rontegenunter-suchungen an Ceroxyden," J. Inorg. Nucl. Chem., 16, 87-99, 1960.

18. Brauer, G., Gingerich, K. A. and Holtschmidt, H., "Uber die Oxyde des Cers-IV, Die Sauerstoffzersetzungdrucke im System der Ceroxyde," J. Inorg. Nucl. Chem., 16, 77-87, 1960.

19. Brauer, G. and Gingerick, K., "The Influence of Temperature on the Cerium Oxide System CeO_2-Ce_2O_3," Rare Earth Research edited by E. Kleber, MacMillian Co., New York, 1961.

20. Kuznetsov, F. A., Beliy, V. I., and Rezukhina, T. N., "Thermodynamic Properties of Cerium Dioxide," (in Russian), Dokl. Akad. Nauk. SSSR, 139, 1405-1408, 1961

21. Bevan, D. J. M. and Kardis, J., "Mixed Oxides of the Type MO_2 (Fluorite) - M_2O_3 - I," J. Inorg. Nucl. Chem., 26, 1509-1523, 1964.

22. Kafstad, P. and Hed, A. Z., "Defect Structure Model for Nonstoichiometric CeO_2," J. Am. Cer. Soc., 50, 681-682, 1967.

23. Ackermann, R. J. and Rauh, E. G., "A High Temperature Study of the Stoichiometry, Phase Behavior, Vaporization Characteristics and Thermodynamic Properties of the Cerium + Oxygen System," J. Chem. Thermodynamics, 3, 609-624, 1971.

24. Panlener, R. J., "A Study of the Defect Strucutre of Pure and Calcia Doped Nonstoichiometric Cerium Dioxide," Ph. D. dissertation, Marquette University, Milwaukee, Wisconsin, 1972.

25. Panlener, R. J., Blumenthal, R. N., and Garnier, J. E., "A Thermodynamic Study of Nonstoichiometric Cerium Dioxide," J. Phys. Chem. Solids, 36, 1213-1222, 1975.

26. Cherepanor, A. M. and Tresvalskii, Highly Refractory Materials and Objects Made from Oxides, (in Russian) Metallurgizdat, Moscow, 1964, p. 358.

27. Trombe, F., "Les Oxydes Super-Refractaires," B. Soc. Fran. Ceramique, 3, 18-26.

28. Ryshkewitch, E., Oxide Ceramics, Academic Press, New York, 1960.

29. Kogan, B. I., Economic Outlines of the Rare Earths, (in Russian), Izd. ANSSSR Moscow, 1961.

30. Wartenberg, V. H. and Gurr, W., "Schmelzdiagramme Hochstfeuerfester Oxyde III," Z. Anorg U. Allge. Chemic., 196, 374-383, 1931.

31. Kaye, G. W. C. and Laby, T. H., Tables of Physical and Chemical Constants, Longman, New York, 1973.

32. Foex, M., "Mesure des Points de Solidification des Oxydes Refractaires," Rev. Hautes Temper. et Refract., 3, 309-326, 1966.

33. Mordovin, O. A., Timofeeva, N. I., and Drozdova, L. N., "Determination of the Melting Points of Rare Earth Oxides," J. Inorg. Mat., 3, 159-162, 1967, (translated from Russian, originally published in Izv. Akad. Nauk. SSSR, Neorg. Mat., 3, 187-189, 1967.)

34. Ruff, O., "Arbeiten im Gabiet Hoher Temperaturen, I," Z. Anorg. Chem, 82, 397-402, 1913.

35. Friederich, Von E. and Sittig, L., "Herstellung and Eigenschaften Hochschmelzender niederer Oxyde," Z. Anorg. Chem., 145, 127-140, 1925.

36. Pascal, P., Nouveau Traite de Chimie Mineral, Masoon, Paris, 1956.

37. Suchet, J. P., Crystal Chemistry and Semiconduction in Transition Metal Binary Compounds, Academic Press, New York, 1971.

38. JANAF Thermochemical Tables, National Bureau of Standards.

VITA

Michael D. Watson was born in Moline, Illinois March 2, 1947. In 1951 he moved to Huntsville, Alabama where he was educated in the public school system, graduating from Huntsville High School in 1965. He attended Georgia Institute of Technology and received a Bachelor of Ceramic Engineering in 1969. After one year of teaching chemistry at Forest Park (Georgia) Senior High School he returned to Georgia Tech for graduate study. In 1973 he received a Master of Science in Metallurgy after completing the thesis "Stabilized ZrO_2-W Composites Produced by Unidirectional Solidification."